neuroleptics two weeks before the PET measurement. Three neuroleptic-naïve patients satisfying criteria for schizophreniform disorder (duration of illness 1 to 4 months at the time of PET measurement) met criteria for schizophrenia at 6-month follow-up. The patients were recruited from the outpatient units of university-affiliated psychiatric hospitals, psychiatric divisions of general hospitals, and a mental clinic in the urban environments of Tokyo and Chiba prefectures in Japan. Exclusion criteria were current or past substance or cannabis or alcohol abuse, mood disorders, organic brain disease, and medication of antipsychotics, antidepressants, or benzodiazepines or mood stabilizers within two weeks before PET measurement. Five out of 11 subjects were smokers.

Psychopathology was assessed by the Positive and Negative Syndrome Scale (PANSS) (Kay et al., 1987). PANSS was completed by three experienced psychiatrists on the same day as PET measurements was performed. They reviewed the ratings after the interviews, and disagreements were resolved by consensus; the consensus ratings were used in this study. The symptom scores were calculated as the total scores, positive symptom, negative symptom, and general symptom subscores of PANSS. The total PANSS score ranged from 60 to 124 (90.4±19.6, mean±SD), mean positive symptom scores were 24.4±5.1, negative symptom scores were 21.4±6.0, and general symptom scores were 44.6±10.2.

Normal control subjects (12 men, 29.0±10.2 years old) were recruited through notices on bulletin boards at the universities and among the staffs of the affiliated hospitals where the patients had been diagnosed. None of the controls had a history of psychiatric or neurological illness, brain injury, chronic somatic illness, or substance abuse. None had taken any drug including benzodiazepines within two weeks before PET measurements. Seven out of 12 subjects were smokers. All the subjects were examined by T1-weighted magnetic resonance image (MRI) using 1.5 T Philips Gyroscan NT to rule out organic brain diseases. This study was approved by the Ethics and Radiation Safety Committee of the National Institute of Radiological Sciences, Chiba, Japan. Written informed consent was obtained from all subjects.

2.2. PET measurement

[^{11}C]Ro15-4513 was synthesized by *N*-methylation of a corresponding *N*-desmethyl precursor with [^{11}C] methyl iodide. The reaction mixtures were purified by liquid chromatography, eluted with CH_3CN/6mM-phosphoric acid=175/325. The radiochemical purities were more than 95%.

The PET system used was ECAT EXACT HR+(CTI-Siemens, Knoxville, TN, USA), which provides 63 planes and a 15.5-cm field of view and was used in 3-dimensional mode. After a 10-minute transmission scan, a bolus of 352.3±66.9 MBq (mean±SD) of [^{11}C] Ro15-4513 with high specific radioactivities (103.4±38.9 GBq/μmol; mean±SD) was injected into the antecubital vein with a 20-ml saline flush. Radioactivity in the brain was measured in a series of sequential frames up to 60 min (total 28 frames).

2.3. PET data analysis

All emission scans were reconstructed with a Hanning filter cut-off frequency of 0.4 (FWHM 7.5 mm). Regions-of-interest (ROIs) were delineated on PET/MRI coregistered images for ten target regions (anterior cingulate, hippocampus, amygdala, thalamus, temporal cortex, prefrontal cortex, insula, caudate, putamen, cerebellum) and the pons as a reference region. Regional binding potentials were calculated using a simplified reference tissue model (SRTM)(Lammertsma and Hume, 1996). In brief, based on the three-compartment model, regional radioactivities in a target region (C_T) can be described by the following equation:

$$C_T(t) = R_1 C_R(t) + (k_2 - R_1\theta_3) C_R(t) * e^{-\theta_3 t},$$

where C_R represents the radioactivity in the reference region, R_1 is the ratio of K_1 in a target region to the reference region, $\theta_3 = k_2/(1+BP)$, K_1 and k_2 are rate constants corresponding to the influx and efflux rates from plasma to the tissue compartments, and * is the

Table 2
Binding potentials for regions of interest

	BP values		*T* test (df=21)	
	Controls (*N*=12)	Patients (*N*=11)	*T* score	*p*
Anterior cingulated	6.08±0.72	6.14±0.63	−0.213	0.833
Hippocampus	5.43±0.77	4.95±0.80	1.432	0.167
Amygdala	5.49±0.56	5.25±0.48	1.118	0.276
Thalamus	2.00±0.28	1.83±0.24	1.534	0.14
Temporal cortex	4.20±0.52	4.12±0.38	0.438	0.666
Prefrontal cortex	3.60±0.35	3.59±0.34	0.09	0.929
Insula	5.79±0.63	5.56±0.46	1.011	0.324
Caudate	2.99±0.43	3.32±0.81	−1.199	0.249
Putamen	2.86±0.36	3.10±0.45	−1.445	0.165
Cerebellum	1.32±0.25	1.34±0.23	0.148	0.883

Values are mean±SD.

convolution operator. In this study, the pons was chosen as the reference tissue because this region is almost devoid of $GABA_A$/BZ receptor complex (Abadie et al., 1992).

2.4. Statistical analysis

Statistical analysis of the difference of regional BP or R_1 for each ROI between patients and controls was performed by repeated measures analysis of variance (ANOVA). When any interaction was found, post hoc Bonferroni correction was used for multiple comparisons. $p<0.05$ was considered significant.

Correlations between regional BP and PANSS scores were analyzed with Pearson's correlation method. $p<0.05$ was considered significant.

3. Results

Regarding regional BP values of [^{11}C]Ro15-4513, two-way repeated ANOVA revealed significant group-region interaction [$F_{4.3,90.6}=2.6$, $p=0.037$]. However, post hoc Bonferroni correction showed no significant differences of BPs for 10 ROIs between patients and controls (Table 2). As for R_1 values, two-way repeated ANOVA revealed no significant main effect of the groups [$F_{4.9,103.9}=1.613$, $p=0.164$] nor group-region interaction [$F_{1,21}=1.532$, $p=0.229$].

For the reference tissue, time activity curves of the pons between patients with schizophrenia and controls were compared with repeated-measures ANOVA with Green–Geisser correction. There was no significant main effect of groups [$F_{1,21}=1.027$, $p=0.323$] or no significant group by time interaction [$F_{2.09,43.9}=0.203$, $p=0.826$].

Regarding the relation to clinical symptoms, there were significant negative correlations between [^{11}C]Ro15-4513 binding in the prefrontal cortex and negative symptom scores ($R=-0.733$, $p=0.010$)(Fig. 1A), general symptom scores ($R=-0.655$, $p=0.029$) (Fig. 1C), and total PANSS scores ($R=-0.690$, $p=0.019$) (Fig. 1D). There was also a negative correlation between [^{11}C]Ro15-4513 binding in the hippocampus and negative symptom scores ($R=-0.605$, $p=0.048$) (Fig. 1B). No other regions

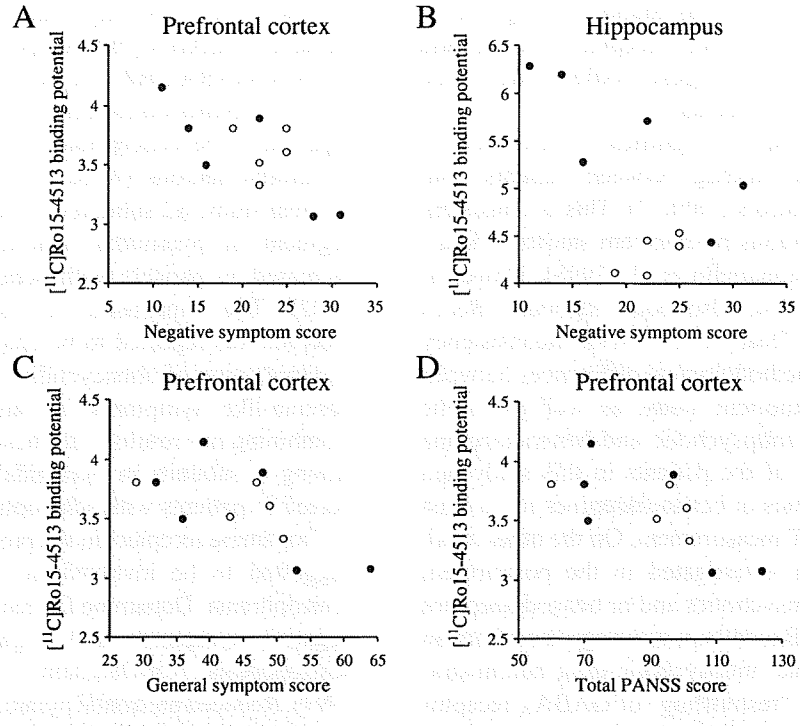

Fig. 1. Relationship between regional [^{11}C]Ro15-4513 binding potentials and PANSS scores in 11 patients with schizophrenia. Filled circles indicate neuroleptic-naïve patients ($N=6$). Open circles indicate drug-free patients ($N=5$). Total PANSS scores consist of positive symptom scores, negative symptom scores, and total symptom scores. There were significant negative correlations between [^{11}C]Ro15-4513 binding in the prefrontal cortex and negative symptom scores ($R=-0.733$, $p=0.010$)(A), general symptom scores ($R=-0.655$, $p=0.029$) (C), and total PANSS scores ($R=-0.690$, $p=0.019$) (D). There was also a negative correlation between [^{11}C]Ro15-4513 binding in the hippocampus and negative symptom scores ($R=-0.605$, $p=0.048$) (B).

Table 3
Correlation between regional [11C]Ro15-4513 binding potentials and PANSS scores

	Positive symptoms		Negative symptoms		General symptoms		Total scores	
Region	*R*	*p*	*R*	*p*	*R*	*p*	*R*	*p*
Anterior cingulate	−0.123	0.718	−0.312	0.350	−0.079	0.817	−0.169	0.620
Hippocampus	−0.008	0.982	−0.605	0.048*	−0.221	0.513	−0.302	0.367
Amygdale	−0.394	0.231	−0.307	0.359	−0.282	0.401	−0.343	0.302
Thalamus	−0.298	0.373	−0.163	0.633	0.005	0.987	−0.125	0.714
Temporal cortex	−0.415	0.205	−0.594	0.054	−0.564	0.070	−0.583	0.060
Prefrontal cortex	−0.485	0.131	−0.733	0.010*	−0.655	0.029*	−0.690	0.019*
Insula	−0.146	0.668	−0.541	0.085	−0.281	0.403	−0.349	0.292
Caudate	−0.164	0.630	−0.118	0.729	0.031	0.929	−0.063	0.854
Putamen	−0.383	0.245	−0.287	0.393	−0.184	0.587	−0.283	0.398
Cerebellum	0.057	0.868	−0.120	0.725	−0.010	0.976	−0.027	−0.937

showed significant correlation with clinical symptom scores (Table 3).

4. Discussion

In this study, significant negative correlation between clinical symptoms (especially negative symptoms) and $GABA_A$/BZ receptor binding in the prefrontal cortex (Fig. 1A, C, D) and the hippocampus (Fig. 1B) of the patients with schizophrenia was found. The significant relation between $GABA_A$/BZ receptor binding and clinical symptoms would suggest dysfunctions of the GABA system in schizophrenia.

Our results showed no significant difference of $GABA_A$/BZ receptor binding between patients with schizophrenia and controls (Table 2). This is consistent with some of the previous postmortem studies (Akbarian et al., 1995; Impagnatiello et al., 1998). However, inconsistent results have also been reported (Benes et al., 1996a, 1996b; Dean et al., 1999). Inconsistency can be attributed to methodological differences between PET study and postmortem study, as well as to the effects of prolonged antipsychotic and benzodiazepine administration. None of the patients in this study had taken any antipsychotics or benzodiazepines for at least two weeks before PET measurement. On the other hand, most of the subjects investigated in the postmortem studies had taken antipsychotics and/or benzodiazepines on a long-term basis. Recently, it was suggested from an animal experiment that antipsychotic drug administration would result in a "reshuffling" of $GABA_A$ receptor subtypes (Skilbeck et al., 2007).

Although there was no significant difference in [^{11}C] Ro15-4513 binding between patients and controls, [^{11}C] Ro15-4513 binding was found to be negatively correlated with clinical symptom scores. Although some previous SPECT studies using [^{123}I]iomazenil showed no significant difference of benzodiazepine binding between patients and controls (Abi-Dargham et al., 1999, Verhoeff et al., 1999), some reported that there were significant negative correlations between benzodiazepine binding and the severity of negative symptoms (Busatto et al., 1997), or cognitive impairment (Ball et al., 1998) in patients with schizophrenia. Our results were consistent with those studies, despite [^{11}C]Ro15-4513 having relatively high affinity for α5 subunit of $GABA_A$/BZ receptor while [^{123}I]iomazenil binds to $GABA_A$/BZ receptor non-selectively.

α5 subunit-containing $GABA_A$ receptors are reported to be concentrated in the apical dendrites of pyramidal neurons (Akbarian et al., 1995). In a postmortem study, α2 subunit of GABA in the axonal initial segment of pyramidal neurons was reported to be increased in patients with schizophrenia (Volk et al., 2002). The expression of subunits of $GABA_A$/BZ receptor was reported to be changed following chronic administration of phencyclidine, which induces schizophrenia-like symptoms in rats (Abe et al., 2000). Combining our results with these reports, the imbalance among α subunits in pyramidal neurons could be expected in patients with schizophrenia.

Dopamine receptors in the prefrontal cortex have been suggested to be involved in the pathophysiology of schizophrenia. Dopamine D1 receptor plays a key role in negative symptoms and cognitive dysfunctions of schizophrenia (Abi-Dargham et al., 2002; Okubo et al., 1997). Reduced prefrontal pyramidal neuron output could change the activity of dopamine neurons in the prefrontal cortex in schizophrenia (Lewis and Gonzalez-Burgos, 2006). The possible change of α5 subunit in the prefrontal cortex might cause the change of pyramidal neuron output, which might interact with dopamine D1 receptor.

Not only the prefrontal cortex but also the hippocampus was found to be correlated negatively with negative symptoms of patients with schizophrenia in this study (Fig. 1B). Hippocampal-dependent spatial learning was improved in α5 subunit of $GABA_A$ receptor-knockout mice (Collinson et al., 2002), or by systemic treatment of an inverse agonist selective for α5 $GABA_A$ receptors (Chambers et al., 2003). The change of α5 subunit of $GABA_A$ receptors in the prefrontal cortex in patients with schizophrenia might affect hippocampal function because of the plastic neuronal connections between the hippocampus and prefrontal cortex (Goldman-Rakic et al., 1984; Laroche et al., 2000; Maccotta et al., 2007; Tierney et al., 2004; Takahashi et al., 2007).

There has been some interest in treating negative symptoms and cognitive dysfunctions in schizophrenia with GABA-modulating drugs (Guidotti et al., 2005; Lewis et al., 2004; Menzies et al., 2007). Imidazenil, which selectively allosterically modulates cortical $GABA_A$ receptors containing α5 subunit, was reported to contribute to amelioration of the behavioral deficits without producing sedation or tolerance liability in mice (Guidotti et al., 2005), and it increased locomotor activity in a social isolation mouse model (Pinna et al., 2006).

There were several limitations to this preliminary study. The number of subjects was small, and five of the eleven patients were previously treated. Further study would be needed with a larger population of drug-naïve patients. Although age correction was not performed, we previously reported no significant age effect of [^{11}C] Ro15-4513 binding (Suhara et al., 1993). We also compared with age-matched subgroup of drug naïve paitents (N=6) with controls (N=12) and two-way repeated ANOVA revealed no significant group-region interaction of [^{11}C]Ro15-4513 binding.

Sex was not matched between patients and controls, but sex differences of [^{11}C]Ro15-4513 binding have not been reported.

In conclusion, the present study showed that [^{11}C] Ro15-4513 binding was negatively correlated with negative symptom scores in schizophrenia. $GABA_A$/BZ receptor including α5 subunit might be involved in the pathophysiology of schizophrenia with negative symptoms.

Role of funding source

This study was supported by a consignment expense for Molecular Imaging Program on "Research Base for PET Diagnosis" from the Ministry of Education, Culture, Sports, Science and Technology (MEXT), Japanese Government. The Ministry had no further role in study design; in the collection, analysis and interpretation of data; in the writing of the report; and in the decision to submit the paper for publication.

Contributors

Y Asai, T Takano and T Suhara designed the study and wrote the protocol. Y Okubo, M Matsuura, A Otsuka, H Takahashi, T Ando, and S Ito recruited the subjects and made psychiatric evaluations. Y Asai, T Takano, and R Arakawa performed the data analysis. Y Asai wrote the first draft of the manuscript. H Ito gave fruitful comments to finalize the manuscript. All authors contributed to and have approved the final manuscript.

Conflict of interest

All the authors have no conflict of interest.

Acknowledgments

We thank Takashi Okauchi for his help with the statistical analysis of PET data, and all the PET members in National Institute of Radiological Sciences for their assistant.

References

Abadie, P., Baron, J.C., Bisserbe, J.C., Boulenger, J.P., Rioux, P., Travere, J.M., et al., 1992. Central benzodiazepine receptors in human brain: estimation of regional Bmax and KD values with positron emission tomography. Eur. J. Pharmacol. 213 (1), 107–115.

Abe, S., Suzuki, T., Ito, T., Baba, A., Hori, T., Kurita, H., et al., 2000. Differential expression of $GABA_A$ receptor subunit mRNAs and ligand binding sites in rat brain following phencyclidine administration. Synapse 38 (1), 51–60.

Abi-Dargham, A., Laruelle, M., Krystal, J., D'Souza, C., Zoghbi, S., Baldwin, R.M., et al., 1999. No evidence of altered in vivo benzodiazepine receptor binding in schizophrenia. Neuropsychopharmacology 20 (6), 650–661.

Abi-Dargham, A., Mawlawi, O., Lombardo, I., Gil, R., Martinez, D., Huang, Y., et al., 2002. Prefrontal dopamine D1 receptors and working memory in schizophrenia. J. Neurosci. 22 (9), 3708–3719.

Akbarian, S., Huntsman, M.M., Kim, J.J., Tafazzoli, A., Potkin, S.G., Bunney Jr, W.E., Jones, E.G., 1995. $GABA_A$ receptor subunit gene expression in human prefrontal cortex: comparison of schizophrenics and controls. Cereb. Cortex 5 (6), 550–560.

Asai Y., Ikoma Y., Takano A., Maeda J., Toyama H., Yasuno F., et al. in press. Quantitative analyses of [^{11}C]Ro15-4513 binding to subunits of $GABA_A$/Benzodiazepine receptor in living human brain. Nucl. Med. Commun.

Ball, S., Busatto, G.F., David, A.S., Jones, S.H., Hemsley, D.R., Pilowsky, L.S., et al., 1998. Cognitive functioning and GABAA/benzodiazepine receptor binding in schizophrenia: a ^{123}I-iomazenil SPET study. Biol. Psychiatry 43 (2), 107–117.

Barnard, E.A., Skolnick, P., Olsen, R.W., Mohler, H., Sieghart, W., Biggio, G., et al., 1998. Subtypes of gamma-aminobutyric acid A receptors: classification on the basis of subunit structure and receptor function. Pharmacol Rev. 50 (2), 291–313.

Benes, F.M., Vincent, S.L., Alsterberg, G., Bird, E.D., SanGiovanni, J.P., 1992. Increased $GABA_A$ receptor binding in superficial layers of cingulate cortex in schizophrenics. J. Neurosci. 12 (3), 924–929.

Benes, F.M., Khan, Y., Vincent, S.L., Wickramasinghe, R., 1996a. Differences in the subregional and cellular distribution of $GABA_A$ receptor binding in the hippocampal formation of schizophrenic brain. Synapse 22 (4), 338–349.

Benes, F.M., Vincent, S.L., Marie, A., Khan, Y., 1996b. Up-regulation of $GABA_A$ receptor binding on neurons of the prefrontal cortex in schizophrenic subjects. Neuroscience 75 (4), 1021–1031.

Busatto, G.F., Pilowsky, L.S., Costa, D.C., Ell, P.J., David, A.S., Lucey, J.V., Kerwin, R.W., 1997. Correlation between reduced in vivo benzodiazepine receptor binding and severity of psychotic symptoms in schizophrenia. Am. J. Psychiatry 154 (1), 56–63.

Chambers, M.S., Atack, J.R., Broughton, H.B., Collinson, N., Cook, S., Dawson, G.R., et al., 2003. Identification of a novel, selective $GABA_A$ alpha5 receptor inverse agonist which enhances cognition. J. Med. Chem. 46 (11), 2227–2240.

Collinson, N., Kuenzi, F.M., Jarolimek, W., Maubach, K.A., Cothliff, R., Sur, C., et al., 2002. Enhanced learning and memory and altered GABAergic synaptic transmission in mice lacking the alpha 5 subunit of the $GABA_A$ receptor. J. Neurosci. 22 (13), 5572–5580.

Crestani, F., Low, K., Keist, R., Mandelli, M., Mohler, H., Rudolph, U., 2001. Molecular targets for the myorelaxant action of diazepam. Mol. Pharmacol. 59 (3), 442–445.

Dean, B., Hussain, T., Hayes, W., Scarr, E., Kitsoulis, S., Hill, C., et al., 1999. Changes in serotonin2A and $GABA_A$ receptors in schizophrenia: studies on the human dorsolateral prefrontal cortex. J. Neurochem. 72 (4), 1593–1599.

Goldman-Rakic, P.S., Selemon, L.D., Schwartz, M.L., 1984. Dual pathways connecting the dorsolateral prefrontal cortex with the hippocampal formation and parahippocampal cortex in the rhesus monkey. Neuroscience 12 (3), 719–743.

Guidotti, A., Auta, J., Davis, J.M., Dong, E., Grayson, D.R., Veldic, M., et al., 2005. GABAergic dysfunction in schizophrenia: new treatment strategies on the horizon. Psychopharmacology (Berl) 180 (2), 191–205.

Halldin, C., Farde, L., Litton, J.E., Hall, H., Sedvall, G., 1992. [^{11}C]Ro 15-4513, a ligand for visualization of benzodiazepine receptor binding. Psychopharmacology 108 (1-2), 16–22.

Impagnatiello, F., Guidotti, A.R., Pesold, C., Dwivedi, Y., Caruncho, H., Pisu, M.G., et al., 1998. A decrease of reelin expression as a putative vulnerability factor in schizophrenia. Proc. Natl. Acad. Sci. U. S. A. 95 (26), 15718–15723.

Inoue, O., Suhara, T., Itoh, T., Kobayashi, K., Suzuki, K., Tateno, Y., 1992. In vivo binding of [^{11}C]Ro15-4513 in human brain measured with PET. Neurosci. Lett. 145 (2), 133–136.

Ishikawa, M., Mizukami, K., Iwakiri, M., Hidaka, S., Asada, T., 2004. Immunohistochemical and immunoblot study of $GABA_A$ alpha1 and beta2/3 subunits in the prefrontal cortex of subjects with schizophrenia and bipolar disorder. Neurosci. Res. 50 (1), 77–84.

Kay, S.R., Fiszbein, A., Opler, L.A., 1987. The positive and negative syndrome scale (PANSS) for schizophrenia. Schizophr. Bull. 13 (2), 261–276.

Laroche, S., Davis, S., Jay, T.M., 2000. Plasticity at hippocampal to prefrontal cortex synapses: dual roles in working memory and consolidation. Hippocampus 10 (4), 438–446.

Lammertsma, A.A., Hume, S.P., 1996. Simplified reference tissue model for PET receptor studies. NeuroImage 4 (3 Pt 1), 153–158.

Lewis, D.A., Gonzalez-Burgos, G., 2006. Pathophysiologically based treatment interventions in schizophrenia. Nat. Med. 12 (9), 1016–1022.

Lewis, D.A., Pierri, J.N., Volk, D.W., Melchitzky, D.S., Woo, T.U., 1999. Altered GABA neurotransmission and prefrontal cortical dysfunction in schizophrenia. Biol. Psychiatry 46 (5), 616–626.

Lewis, D.A., Volk, D.W., Hashimoto, T., 2004. Selective alterations in prefrontal cortical GABA neurotransmission in schizophrenia: a novel target for the treatment of working memory dysfunction. Psychopharmacology (Berl) 174 (1), 143–150.

Lingford-Hughes, A., Hume, S.P., Feeney, A., Hirani, E., Osman, S., Cunnungham, V.J., et al., 2002. Imaging the GABA-benzodiazepine receptor subtype containing the α5-subunit *in vivo* with [^{11}C]Ro15 4513 positron emission tomography. J. Cereb. Blood Flow Metab. 22 (7), 878–889.

Low, K., Crestani, F., Keist, R., Benke, D., Brunig, I., Benson, J.A., et al., 2000. Molecular and neuronal substrate for the selective attenuation of anxiety. Science 290 (5489), 131–134.

Lüddens, H., Seeburg, P.H., Korpi, E.R., 1994. Impact of beta and gamma variants on ligand-binding properties of gamma-aminobutyric acid type A receptors. Mol. Pharmacol. 45 (5), 810–814.

Lüddens, H., Korpi, E.R., Seeburg, P.H., 1995. $GABA_A$/benzodiazepine receptor heterogeneity: neurological implications. Neuropharmacology 34 (3), 245–254.

Maccotta, L., Buckner, R.L., Gilliam, F.G., Ojemann, J.G., 2007. Changing frontal contributions to memory before and after medial temporal lobectomy. Cereb. Cortex 17 (2), 443–456.

Maeda, J., Suhara, T., Kawabe, K., Okauchi, T., Obayashi, S., Hojo, J., Suzuki, K., 2003. Visualization of alpha5 subunit of $GABA_A$/benzodiazepine receptor by [^{11}C]Ro15-4513 using positron emission tomography. Synapse 47 (3), 200–208.

Mehta, A.K., Ticku, M.K., 1999. An update on $GABA_A$ receptors. Brain Res. Brain Res. Rev. 29, 196–217.

Menzies, L., Ooi, C., Kamath, S., Suckling, J., McKenna, P., Fletcher, P., et al., 2007. Effects of gamma-aminobutyric acid-modulating drugs on working memory and brain function in patients with schizophrenia. Arch. Gen. Psychiatry 64 (2), 156–167.

Mohler, H., Crestani, F., Rudolph, U., 2001. $GABA_A$-receptor subtypes: a new pharmacology. Curr. Opin. Pharmacol. 1 (1), 22–25.

Moss, S.J., Smart, T.G., 2001. Constructing inhibitory synapses. Nat. Rev. Neurosci. 2 (4), 240–250.

Ohnuma, T., Augood, S.J., Arai, H., McKenna, P.J., Emson, P.C., 1999. Measurement of GABAergic parameters in the prefrontal cortex in schizophrenia: focus on GABA content, $GABA_A$ receptor alpha-1 subunit messenger RNA and human GABA transporter-1 (HGAT-1) messenger RNA expression. Neuroscience 93 (2), 441–448.

Okubo, Y., Suhara, T., Suzuki, K., Kobayashi, K., Inoue, O., Terasaki, O., et al., 1997. Decreased prefrontal dopamine D_1 receptors in schizophrenia revealed by PET. Nature 385 (6617), 634–636.

Pappata, S., Samson, Y., Chavoix, C., Prenant, C., Maziere, M., Baron, J.C., 1988. Regional specific binding of [^{11}C]Ro15 1788 to central type benzodiazepine receptors in human brain: quantitative evaluation by PET. J. Cereb. Blood Flow Metab. 8 (3), 304–313.

Pinna, G., Agis-Balboa, R.C., Zhubi, A., Matsumoto, K., Grayson, D.R., Costa, E., Guidotti, A., 2006. Imidazenil and diazepam increase locomotor activity in mice exposed to protracted social isolation. Proc. Natl. Acad. Sci. U. S. A. 103 (11), 4275–4280.

Reynolds, G.P., Czudek, C., Andrews, H.B., 1990. Deficit and hemispheric asymmetry of GABA uptake sites in the hippocampus in schizophrenia. Biol. Psychiatry 27 (9), 1038–1044.

Serwanski, D.R., Miralles, C.P., Christie, S.B., Mehta, A.K., Li, X., De Blas, A.L., 2006. Synaptic and nonsynaptic localization of GABAA receptors containing the alpha5 subunit in the rat brain. J. Comp. Neurol. 499 (3), 458–470.

Simpson, M.D., Slater, P., Deakin, J.F., Royston, M.C., Skan, W.J., 1989. Reduced GABA uptake sites in the temporal lobe in schizophrenia. Neurosci. Lett. 107 (1-3), 211–215.

Skilbeck, K.J., O'Reilly, J.N., Johnston, G.A., Hinton, T., 2007. The effects of antipsychotic drugs on $GABA_A$ receptor binding depend on period of drug treatment and binding site examined. Schizophr. Res. 90 (1-3), 76–80.

Suhara, T., Inoue, O., Kobayashi, K., Suzuki, K., Itoh, T., Tateno, Y., 1993. No age-related changes in human benzodiazepine receptor binding measured by PET with [^{11}C]Ro15-4513. Neurosci. Lett. 159 (1-2), 207–210.

Takahashi, H., Kato, M., Hayashi, M., Okubo, Y., Takano, A., Ito, H., Suhara, T., 2007. Memory and frontal lobe functions; possible relations with dopamine D_2 receptors in the hippocampus. NeuroImage 34 (4), 1643–1649.

Tierney, P.L., Degenetais, E., Thierry, A.M., Glowinski, J., Gioanni, Y., 2004. Influence of the hippocampus on interneurons of the rat prefrontal cortex. Eur. J. Neurosci. 20 (2), 514–524.

Tobler, I., Kopp, C., Deboer, T., Rudolph, U., 2001. Diazepam-induced changes in sleep: role of the alpha 1 $GABA_A$ receptor subtype. Proc. Natl. Acad. Sci. U. S. A. 98 (11), 6464–6469.

Verhoeff, N.P., Soares, J.C., D'Souza, C.D., Gil, R., Degen, K., Abi-Dargham, A., et al., 1999. [^{123}I]Iomazenil SPECT benzodiazepine receptor imaging in schizophrenia. Psychiatry Res. 91 (3), 163–173.

Volk, D.W., Pierri, J.N., Fritschy, J.M., Auh, S., Sampson, A.R., Lewis, D.A., 2002. Reciprocal alterations in pre- and postsynaptic inhibitory markers at chandelier cell inputs to pyramidal neurons in schizophrenia. Cereb. Cortex 12 (10), 1063–1070.

Wieland, H.A., Lüddens, H., 1994. Four amino acid exchanges convert a diazepam-insensitive, inverse agonist-preferring $GABA_A$ receptor into a diazepam-preferring $GABA_A$ receptor. J. Med. Chem. 37 (26), 4576–4580.

Quantitative Analysis of Norepinephrine Transporter in the Human Brain Using PET with (S,S)-^{18}F-FMeNER-D_2

Ryosuke Arakawa[1,2], Masaki Okumura[1,2], Hiroshi Ito[1], Chie Seki[1], Hidehiko Takahashi[1], Harumasa Takano[1], Ryuji Nakao[3], Kazutoshi Suzuki[3], Yoshiro Okubo[2], Christer Halldin[4], and Tetsuya Suhara[1]

[1]Molecular Neuroimaging Group, Molecular Imaging Center, National Institute of Radiological Sciences, Chiba, Japan; [2]Department of Neuropsychiatry, Nippon Medical School, Tokyo, Japan; [3]Molecular Probe Group, Molecular Imaging Center, National Institute of Radiological Sciences, Chiba, Japan; and [4]Psychiatry Section, Department of Clinical Neuroscience, Karolinska Institutet, Karolinska Hospital, Stockholm, Sweden

(S,S)-^{18}F-FMeNER-D_2 was recently developed as a radioligand for the measurement of norepinephrine transporter imaging with PET. In this study, a norepinephrine transporter was visualized in the human brain using this radioligand with PET and quantified by several methods. **Methods:** PET scans were performed on 10 healthy men after intravenous injection of (S,S)-^{18}F-FMeNER-D_2. Binding potential relative to nondisplaceable binding (BP_{ND}) was quantified by the indirect kinetic, simplified reference-tissue model (SRTM), multilinear reference-tissue model (MRTM), and ratio methods. The indirect kinetic method was used as the gold standard and was compared with the SRTM method with scan times of 240 and 180 min, the MRTM method with a scan time of 240 min, and the ratio method with a time integration interval of 120–180 min. The caudate was used as reference brain region. **Results:** Regional radioactivity was highest in the thalamus and lowest in the caudate during PET scanning. BP_{ND} values by the indirect kinetic method were 0.54 ± 0.19 and 0.35 ± 0.25 in the thalamus and locus coeruleus, respectively. BP_{ND} values found by the SRTM, MRTM, and ratio methods agreed with the values demonstrated by the indirect kinetic method (r = 0.81–0.92). **Conclusion:** The regional distribution of (S,S)-^{18}F-FMeNER-D_2 in our study agreed with that demonstrated by previous PET and postmortem studies of norepinephrine transporter in the human brain. The ratio method with a time integration interval of 120–180 min will be useful for clinical research of psychiatric disorders for estimation of norepinephrine transporter occupancy by antidepressants without requiring arterial blood sampling and dynamic PET.

Key Words: norepinephrine transporter; (S,S)-^{18}F-FMeNER-D_2; positron emission tomography; human brain; thalamus

J Nucl Med 2008; 49:1270–1276
DOI: 10.2967/jnumed.108.051292

Norepinephrine, one of the monoamine neurotransmitters in the central nervous system, has been reported to be related to several functions such as memory, cognition, consciousness, and emotion and to play important roles in psychiatric disorders (*1–4*). Norepinephrine transporter is responsible for the reuptake of norepinephrine into presynaptic nerves. Norepinephrine reuptake inhibitors are used for the treatment of depression and attention deficit hyperactivity disorder (ADHD) (*4–7*). Thus, changes in norepinephrine transporter functions in several psychiatric disorders can be expected, but in vivo estimation has not been performed because of a lack of suitable radioligands for norepinephrine transporters.

(S,S)-^{18}F-FMeNER-D_2 has recently been developed as a radioligand for the measurement of norepinephrine transporter for PET (*8*). (S,S)-^{18}F-FMeNER-D_2 is a reboxetine analog and has high affinity for norepinephrine transporter and high selectivity from other monoamine transporters. Tracer distribution and dosimetry of (S,S)-^{18}F-FMeNER-D_2 were reported in monkey (*8,9*) and human studies (*10,11*). Another monkey study showed that (S,S)-^{18}F-FMeNER-D_2 binding decreased by the administration of atomoxetine, a selective norepinephrine reuptake inhibitor (*12*). However, quantitative analyses of (S,S)-^{18}F-FMeNER-D_2 bindings using an arterial input function have not yet, to our knowledge, been performed.

In this study, we aimed to quantify the norepinephrine transporter bindings in the human brain using (S,S)-^{18}F-FMeNER-D_2 with arterial blood sampling and also to validate noninvasive methods for quantification without arterial blood sampling.

MATERIALS AND METHODS

Subjects

Ten healthy men (age range, 21–26 y; mean ± SD, 22.7 ± 1.6 y) participated in this study. All subjects were free of any somatic, neurologic, or psychiatric disorders, and they had no

Received Jan. 30, 2008; revision accepted May 2, 2008.
For correspondence or reprints contact: Hiroshi Ito, Molecular Neuroimaging Group, Molecular Imaging Center, National Institute of Radiological Sciences, 4-9-1, Anagawa, Inage-ku, Chiba, 263-8555, Japan.
E-mail: hito@nirs.go.jp

history of current or previous drug abuse. Written informed consent was obtained from all subjects following a complete description of this study. The study was approved by the Ethics and Radiation Safety Committee of the National Institute of Radiologic Sciences, Chiba, Japan.

PET Procedure

(S,S)-^{18}F-FMeNER-D_2 was synthesized by fluoromethylation of nor-ethyl-reboxetine with ^{18}F-bromofluoromethane-d_2 as previously described (*8*). A PET scanner system (ECAT EXACT HR+; CTI-Siemens) was used for all subjects, with a head holder used to minimize head movement. A transmission scan for attenuation correction was performed using a ^{68}Ge–^{68}Ga source. Dynamic PET scans were performed after a 1-min intravenous slow bolus injection of 353.4–382.7 MBq (mean ± SD, 368.1 ± 9.1 MBq) of (S,S)-^{18}F-FMeNER-D_2. The specific radioactivity of (S,S)-^{18}F-FMeNER-D_2 was 144.8–390.2 GBq/μmol (312.8 ± 76.2 GBq/μmol). Brain radioactivities were measured from 0 to 90 min (1 min × 10, 2 min × 15, and 5 min × 10), from 120 to 180 min (10 min × 6), and from 210 to 240 min (10 min × 3). MR images of the brain were acquired with a 1.5-T MRI scanner (Gyroscan NT; Philips). T1-weighted images were obtained at 1-mm slices.

Arterial Blood Sampling and Metabolite Analysis

To obtain the arterial input function, arterial blood samples were taken manually 42 times during the PET scan. Each blood sample was centrifuged to obtain plasma and blood cell fractions, and the concentrations of radioactivity in whole blood and in plasma were measured.

The percentage of unchanged (S,S)-^{18}F-FMeNER-D_2 in plasma was determined by high-performance liquid chromatography in 22 of the blood samples. Acetonitrile was added to each plasma sample, and samples were centrifuged. The supernatant was subjected to high-performance liquid chromatography radiodetection analysis (column: XBridge Prep C18, mobile phase, 90% acetonitrile/50 mM ammonium acetate = 48/52; Waters). Plasma input function was defined as radioactivity of plasma multiplied by the percentage of unchanged radioligand.

Regions of Interest

All MR images were coregistered to the PET images using a statistical parametric mapping system (SPM2; The Wellcome Trust Centre for Neuroimaging, University College London). Regions of interest were drawn manually on summed PET images, with reference to coregistered MR images, and were defined for the thalamus, locus coeruleus, hippocampus, anterior cingulate gyrus, and caudate head. Regional radioactivity was calculated for each frame, corrected for decay, and plotted versus time.

Kinetic Model of ^{18}F-FMeNER-D_2

To describe the kinetics of (S,S)-^{18}F-FMeNER-D_2 in the brain, the 3-compartment model with 4 first-order rate constants was used. The 3 compartments were defined as follows: C_P was the radioactivity concentration of unchanged radioligand in plasma (arterial input function), C_{ND} was the radioactivity concentration of nondisplaceable radioligand in the brain, including nonspecifically bound and free radioligand, and C_S was the radioactivity concentration of radioligand specifically bound to transporters. The rate constants K_1 and k_2 represent the influx and efflux rates, respectively, for radioligand diffusion through the blood–brain barrier, and the rate constants k_3 and k_4 are the radioligand transfers between the compartments for nondisplaceable and specifically bound radioligand, respectively. This model can be described by the following equations:

$$\frac{dC_{ND}(t)}{dt} = K_1C_P(t) - (k_2+k_3)C_{ND}(t) + k_4C_S(t),$$

$$\frac{dC_S(t)}{dt} = k_3C_{ND}(t) - k_4C_S(t), \text{ and}$$

$$C_T(t) = C_{ND}(t)+C_S(t).$$

$C_T(t)$ is the total radioactivity concentration in any brain region measured by PET.

Calculation of (S,S)-^{18}F-FMeNER-D_2 Binding Potential

(S,S)-^{18}F-FMeNER-D_2 binding was quantified by the indirect kinetic, simplified reference-tissue model (SRTM), multilinear reference-tissue model (MRTM), and ratio methods. In these methods, (S,S)-^{18}F-FMeNER-D_2 bindings were expressed as binding potentials relative to nondisplaceable binding (BP_{ND}) (*13*). We used the caudate as the reference brain region because of its

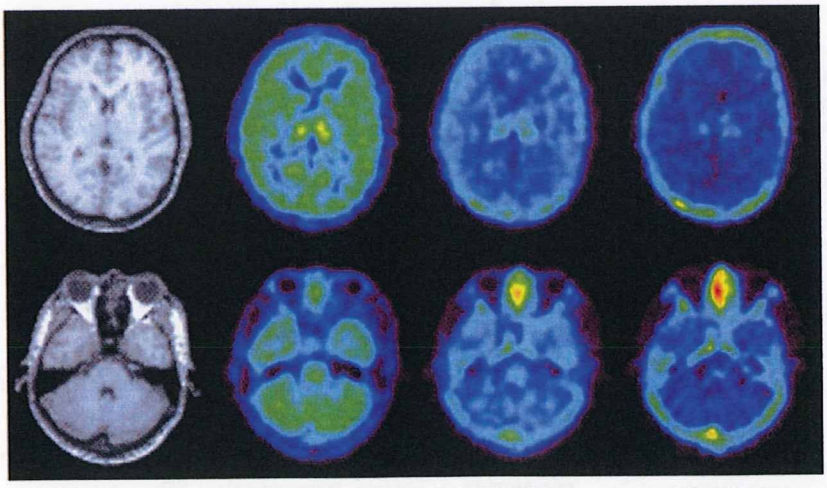

FIGURE 1. Typical summed PET images of (S,S)-^{18}F-FMeNER-D_2 and T1-weighted MR images. Upper panel shows slice of caudate and thalamus, and lower panel shows slice of locus coeruleus.

negligible norepinephrine transporter density (*14–16*). Software (PMOD; PMOD Technologies) was used for these analyses.

Indirect Kinetic Method

With the caudate as reference region, BP_{ND} can be expressed as:

$$BP_{ND} = \frac{V_{T(regions)}}{V_{T(caudate)}} - 1,$$

where $V_{T(regions)}$ is the total distribution volume (= $[K_1/k_2][k_3/k_4 + 1]$) of target regions and $V_{T(caudate)}$ is the total distribution volume of the caudate. The K_1, k_2, k_3, and k_4 values were determined by nonlinear least-squares curve fitting to the regional time–activity curves. In this analysis, blood volume (V_b), which depends on the first-pass extraction fraction of the tracer, was also estimated using the radioactivity of whole blood to diminish the influence of the tracer remaining in the blood. In this study, the indirect kinetic method was used as the standard method (*17*).

SRTM Method

Assuming that both target and reference regions have the same level of nondisplaceable binding, the SRTM method can be used to describe time–activity data in the target region as follows (*18*):

$$C_T(t) = R_1 C_R(t) + \left(k_2 - R_1 \frac{k_2}{1+BP_{ND}}\right) C_R(t) \otimes \exp\left(\frac{-k_2}{1+BP_{ND}} t\right),$$

where R_1 is the ratio of K_1/K_1' (K_1, influx rate constant for the brain region; K_1', influx rate constant for the reference region), $C_R(t)$ is the radioactivity concentration in the reference region (caudate), and $\otimes$ denotes the convolution integral. Using this model, 3 parameters (R_1, k_2, and BP_{ND}) were estimated by a nonlinear curve-fitting procedure. Scan data up to 180 or 240 min were used.

MRTM Method

The MRTM method is one of the variations of the graphical approaches (*19*). After a certain equilibrium time (t*), the following multilinear regression is obtained:

$$C_T(T) = -\frac{V_{T(regions)}}{V_{T(caudate)}} \int_0^T C_R(t)dt + \frac{1}{b} \int_0^T C_T(t)dt - \frac{V_{T(regions)}}{V_{T(caudate)} k_2' b} C_R(T),$$

where k_2' is the efflux rate constant for the reference region. In this analysis, t* was determined so that the maximum error from the regression within the linear segment would be 10% for each time–activity curve. BP_{ND} for the MRTM method was calculated using the same equation as described previously for the indirect kinetic method (= $V_{T(regions)}/V_{T(caudate)} - 1$). Scan data up to 240 min were used.

Ratio Method

In the ratio method, BP_{ND} can be expressed as:

$$BP_{ND} = \frac{AUC_{(regions)}}{AUC_{(caudate)}} - 1,$$

where $AUC_{(regions)}$ is the area under the time–activity curve of the target regions and $AUC_{(caudate)}$ is the area under the time–activity curve of the caudate. The integration interval of 120–180 min was used in this method.

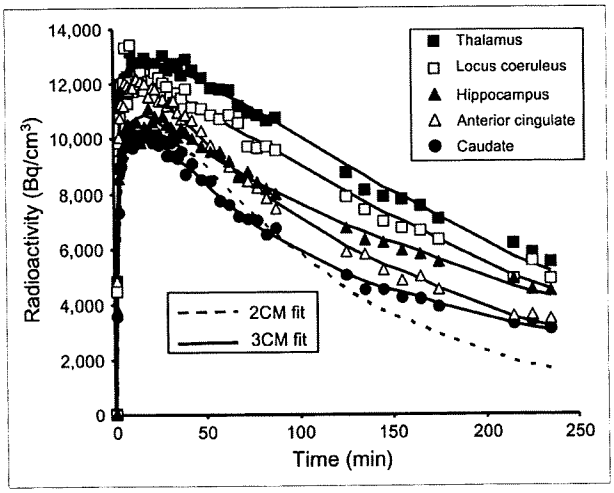

FIGURE 2. Typical time–activity curves of (S,S)-^{18}F-FMeNER-D_2 in brain. Time–activity curves of all regions could be described by 3-compartment model (3CM). Time–activity curve of caudate could also be described by 2-compartment model (2CM).

Simulation Study

A simulation study was performed to estimate errors in BP_{ND} calculated by the SRTM and ratio methods. Tissue time–activity curves for the thalamus were generated using the 3-compartment model. The rate constant values K_1, k_2, and k_4 of the thalamus were assumed to be 0.157, 0.037, and 0.016, respectively. The value of k_3 ranged from 0.019 to 0.039 in 6 steps. Tissue time–activity curves for the caudate were also generated using the 3-compartment model, assuming that the rate constant values K_1, k_2, k_3, and k_4 were 0.124, 0.032, 0.010, and 0.010, respectively. These assumed values were taken from the results obtained by the kinetic approach. The average of arterial input function for all

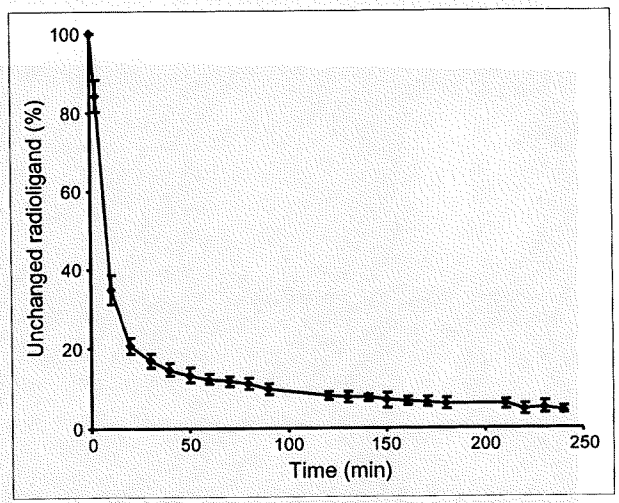

FIGURE 3. Average percentage of unchanged (S,S)-^{18}F-FMeNER-D_2 in plasma. Bars indicate 1 SD.

TABLE 1
Data for Each Brain Region Determined by Kinetic Approach Using 3-Compartment Model with Arterial Input Function

Region	V_b	Rate constant				V_{ND}	V_T
		K_1 (mL/mL/min)	k_2 (min^{-1})	k_3 (min^{-1})	k_4 (min^{-1})		
Thalamus	0.045 ± 0.016	0.157 ± 0.025	0.037 ± 0.005	0.027 ± 0.007	0.016 ± 0.002	4.36 ± 0.90	11.45 ± 2.29
Locus coeruleus	0.032 ± 0.008	0.154 ± 0.026	0.040 ± 0.009	0.020 ± 0.008	0.013 ± 0.004	4.06 ± 1.01	9.89 ± 1.78
Hippocampus	0.038 ± 0.010	0.119 ± 0.013	0.035 ± 0.011	0.022 ± 0.016	0.015 ± 0.005	3.73 ± 0.83	8.48 ± 1.14
Anterior cingulate	0.053 ± 0.011	0.144 ± 0.019	0.032 ± 0.005	0.010 ± 0.005	0.012 ± 0.004	4.61 ± 1.04	8.33 ± 1.70
Caudate (3-compartment model)	0.031 ± 0.008	0.124 ± 0.018	0.032 ± 0.005	0.010 ± 0.005	0.010 ± 0.004	3.92 ± 0.80	7.51 ± 1.51
Caudate (2-compartment model)	0.045 ± 0.010	0.109 ± 0.017	0.019 ± 0.001			5.77 ± 0.98	

Values are mean ± SD. V_{ND} is defined as K_1/k_2 and V_T as $(K_1/k_2)(k_3/k_4 + 1)$.

subjects was used to generate the time–activity curves. With these generated time–activity curves, BP_{ND} values were calculated by the SRTM (scan time of 240 min), MRTM, and ratio methods. The calculated BP_{ND} values for the simulation study were compared with those calculated by the indirect kinetic method.

RESULTS

Typical summed PET images of 3 time periods and T1-weighted MR images are shown in Figure 1. Typical time–activity curves in the brain showed that regional radioactivity was highest in the thalamus and lowest in the caudate (Fig. 2). Time–activity curves for all regions could be described by the 3-compartment model. The time–activity curve for the caudate could also be described by the 2-compartment model. The average percentage of unchanged (S,S)-^{18}F-FMeNER-D_2 in plasma was 84.4% ± 3.9% at 3 min, 35.1% ± 3.7% at 10 min, 10.0% ± 1.4% at 90 min, 6.1% ± 1.3% at 180 min, and 4.5% ± 0.9% at 240 min (Fig. 3).

The blood volume, rate constants, nondisplaceable distribution volume (V_{ND}), and total distribution volume (V_T) for each brain region determined by the kinetic approach using the 3-compartment model with arterial input function are shown in Table 1. For the caudate, the 2-compartment model without a specific binding compartment was also applied. Akaike information criteria of the 3-compartment model were lower than those of the 2-compartment model (143 ± 16 vs. 227 ± 6, $P < 0.0001$; paired t statistics).

The BP_{ND} values of the thalamus calculated by all methods are shown in Table 2. BP_{ND} values in the thalamus by the MRTM method showed the best correlation with those by the indirect kinetic method ($r = 0.92$) (Fig. 4C). The SRTM method with scan times of 180 and 240 min and the ratio method also agreed with the BP_{ND} values by the indirect kinetic method ($r = 0.81$–0.91) (Figs. 4A, 4B, and 4D). However, BP_{ND} values in brain regions other than the thalamus could not be estimated by the SRTM and MRTM methods because of failed curve fitting, showing no convergence. The BP_{ND} values of each brain region by the indirect kinetic and ratio methods are shown in Table 3. The correlation of BP_{ND} values in all target regions between the indirect kinetic and the ratio methods is shown in Figure 5A. The Bland–Altman plot of BP_{ND} values by these 2 methods is shown in Figure 5B.

In the simulation study, estimated BP_{ND} values, compared with assumed BP_{ND} values, by the SRTM (scan time of 240 min), MRTM, and ratio methods were slightly overestimated (Fig. 6).

DISCUSSION

After intravenous injection of (S,S)-^{18}F-FMeNER-D_2, radioactivity was highest in the thalamus and lowest in the caudate. BP_{ND} in the thalamus using the ratio method was 0.67 ± 0.15, almost the same value as found in a previous human PET study (*10*). The locus coeruleus showed relatively high uptake, and the hippocampus and anterior cingulate cortex showed relatively low uptake. This result was in agreement with previous reports that the thalamus and locus coeruleus showed high densities of norepinephrine transporters (*14–16,20*). Previous autoradiographic studies with human postmortem brains reported that norepinephrine transporter density in the locus coeruleus was higher by about 10 times than that in the thalamus (*14,15*). However,

TABLE 2
BP_{ND} Values in Thalamus by All Methods

Method	BP_{ND}
Indirect kinetic	0.54 ± 0.19
SRTM (240 min)	0.61 ± 0.14
SRTM (180 min)	0.64 ± 0.14
MRTM	0.61 ± 0.14
Ratio	0.67 ± 0.15

Values are mean ± SD.

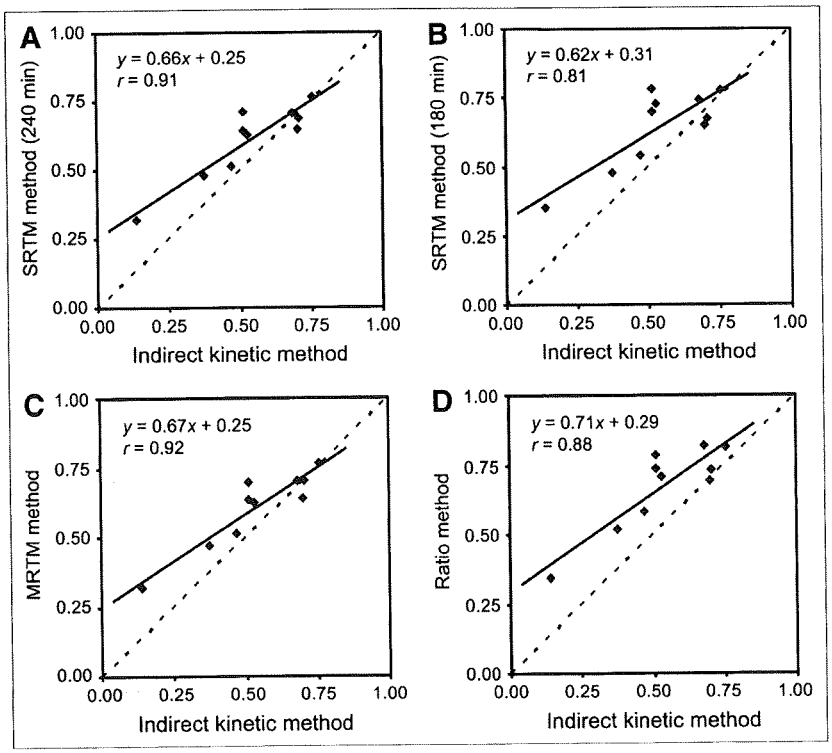

FIGURE 4. Correlation between BP_{ND} values in thalamus estimated by indirect kinetic method and SRTM method with scan time of 240 min (A) or 180 min (B), MRTM method (C), or ratio method (D).

previous and present PET studies reported almost the same values between the locus coeruleus and thalamus (*10,16*). One possible reason for the discrepancy was the partial-volume effect due to the limited spatial resolution of the PET scanner, the locus coeruleus being a very small structure.

In the current study, the indirect kinetic method with arterial blood sampling was used as the standard method (*17*). The BP_{ND} values in the thalamus by the other 3 methods—the SRTM with scan times of 240 and 180 min, MRTM, and ratio methods—were in agreement with those found by the indirect kinetic method. Although the indirect kinetic method was considered the standard method, it required a long PET time as well as arterial blood sampling, an invasive procedure particularly unsuitable for patients with psychiatric disorders. Because the ratio method does not require long PET and arterial blood sampling, this method would be preferable for clinical investigation. The SRTM and MRTM methods can estimate only the thalamus, as curve fitting failed in other brain regions. The MRTM2 method (*19*) may be able to estimate BP_{ND} in regions other than thalamus; however, weighted k_2' value among brain regions could not be calculated in this tracer. The possible reasons of failed curve fitting might be the small differences of time–activity curves between target and reference regions and the noise in time–activity curves. The ratio method could reveal BP_{ND} values in brain regions other than the thalamus. The BP_{ND} values by the ratio method were in agreement with those by the indirect kinetic method for all brain regions (Fig. 5A). Although bias was observed by the ratio method, this bias did not change according to the BP_{ND} values (Fig. 5B). The ratio method could estimate norepinephrine transporter binding in the thalamus and also other brain regions.

The time–activity curves in the caudate were better described by the 3-compartment model than the 2-compartment model. Similar results were reported for several PET radioligands; the kinetics in the reference region were also evaluated using the 3-compartment model (*17,21,22*). The results could be explained if the caudate contained specific binding for norepinephrine transporters. However, previous autoradiographic studies showed that the density of norepinephrine transporters in the caudate was very low (*14–16*). Another possible explanation is that the compartments of free and nonspecific binding could be separated by the kinetic analysis. Moreover, spillover from

TABLE 3
BP_{ND} Values for Each Brain Region by Indirect Kinetic and Ratio Methods

Region	Indirect kinetic method	Ratio method
Thalamus	0.54 ± 0.19	0.67 ± 0.15
Locus coeruleus	0.35 ± 0.25	0.42 ± 0.13
Hippocampus	0.13 ± 0.14	0.23 ± 0.09
Anterior cingulate	0.13 ± 0.16	0.15 ± 0.09

Values are mean ± SD.

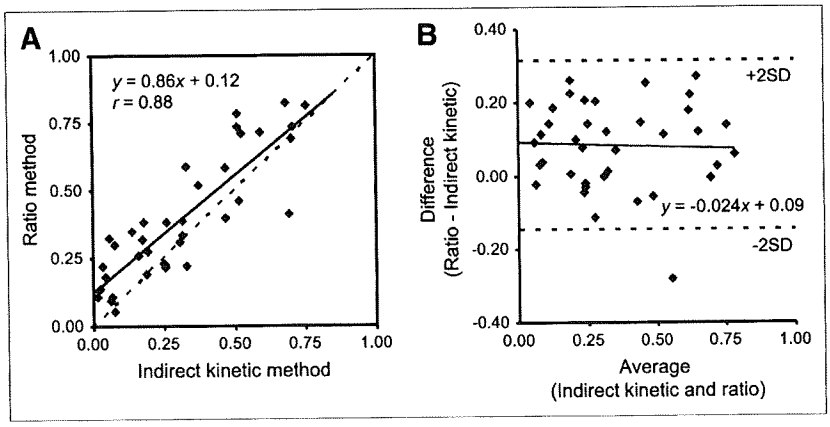

FIGURE 5. Correlation between BP_{ND} values in all target regions estimated by indirect kinetic method and ratio method (A) and Bland–Altman plot (B).

other brain regions to the caudate may affect the results because the caudate is a small structure and is surrounded by regions with specific binding.

In this study, we investigated norepinephrine transporter binding in only limited regions. Other brain regions such as the cerebral cortex and cerebellum are also considered to possess norepinephrine neurons and norepinephrine transporters (*14–16*). However, (S,S)-^{18}F-FMeNER-D_2 showed that defluorination and uptake of ^{18}F in the skull influenced cerebral radioactivity (*8*). Although (S,S)-^{18}F-FMeNER-D_2 had reduced defluorination by the dideuteration, compared with (S,S)-^{18}F-FMeNER, estimation in the cerebral cortex or cerebellum adjacent to the skull was considered difficult.

In this study, occupancy of norepinephrine transporter by antidepressants was not evaluated. Previous animal studies showed dose-dependent norepinephrine transporter occupancy by atomoxetine (*12*). However, a human study using [^{11}C](S,S)-MRB reported no differences in occupancy between different doses of atomoxetine (*16*). Further, occupancy studies in humans to estimate the clinical effects of antidepressants, similar to occupancy studies for dopamine D_2 receptor and serotonin transporters (*23,24*), will be needed.

In the simulation study, BP_{ND} values by the SRTM with a scan time of 240 min, MRTM, and the ratio methods were overestimated, compared with assumed BP_{ND} (Fig. 6). Such overestimation was also observed in measured PET data, especially in regions with low specific binding (Figs. 4A, 4C, and 4D). The degree of overestimation of BP_{ND} was larger in measured data than that in the simulation, especially in regions with low specific binding. Noise in measured data might cause such discrepancy, and therefore further studies using simulated data with added noise may be required. Although linear correlation was observed in BP_{ND} values between the ratio and indirect kinetic methods, this overestimation may cause errors in the calculation of occupancy by antidepressants. When baseline BP_{ND} is 0.6, estimated occupancy by the ratio method is 22%, 43%, and 65%, corresponding to the assumed occupancy of 25%, 50%, and 75%, respectively (Fig. 6). The SRTM and MRTM methods also showed the underestimation of occupancy, 21%, 43%, and 64% by the former and 21%, 42%, and 63% by the latter.

CONCLUSION

(S,S)-^{18}F-FMeNER-D_2 is a suitable radioligand for PET measurement of norepinephrine transporters in the human brain. The 3-compartment model could well describe the brain kinetics of (S,S)-^{18}F-FMeNER-D_2. Because the ratio method does not require long PET imaging times and arterial blood sampling, this method would be useful for clinical research of psychiatric disorders.

ACKNOWLEDGMENTS

We thank Dr. Fumitoshi Kodaka, Dr. Tatsui Otsuka, Katsuyuki Tanimoto, Takahiro Shiraishi, and Akira Ando

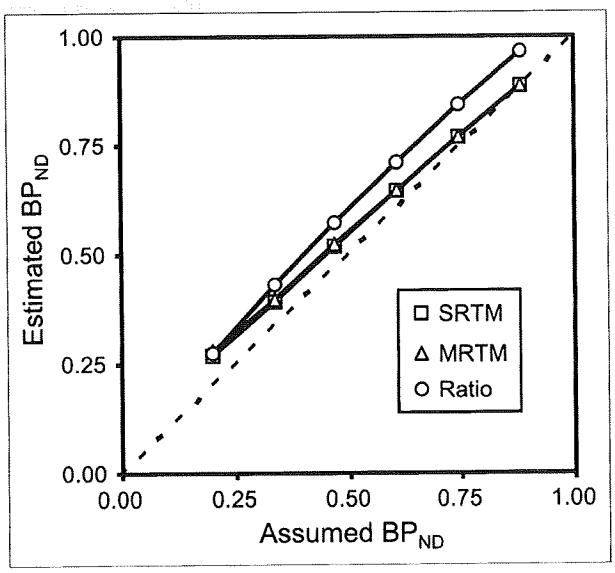

FIGURE 6. Correlations between assumed BP_{ND} values by indirect kinetic method and those by SRTM with scan time of 240 min, MRTM method, or ratio method in simulation studies.

for their assistance in performing the PET experiments at the National Institute of Radiological Sciences. We also thank Yoshiko Fukushima of the National Institute of Radiological Sciences for her help as clinical research coordinator. This study was supported by a consignment expense for the Molecular Imaging Program on Research Base for PET Diagnosis from the Ministry of Education, Culture, Sports, Science and Technology (MEXT), Japanese government, and by a Health and Labor Sciences Research Grant for Research on Psychiatric and Neurological Diseases and Mental Health from the Ministry of Health, Labor and Welfare, Japanese government.

REFERENCES

1. Harmer CJ, Shelley NC, Cowen PJ, Goodwin GM. Increased positive versus negative affective perception and memory in healthy volunteers following selective serotonin and norepinephrine reuptake inhibition. *Am J Psychiatry.* 2004;161:1256–1263.
2. Strange BA, Hurlemann R, Dolan RJ. An emotion-induced retrograde amnesia in humans is amygdala- and beta-adrenergic-dependent. *Proc Natl Acad Sci USA.* 2003;100:13626–13631.
3. Southwick SM, Davis M, Horner B, et al. Relationship of enhanced norepinephrine activity during memory consolidation to enhanced long-term memory in humans. *Am J Psychiatry.* 2002;159:1420–1422.
4. Nutt DJ. The role of dopamine and norepinephrine in depression and antidepressant treatment. *J Clin Psychiatry.* 2006;67(suppl 6):3–8.
5. Cheng JY, Chen RY, Ko JS, Ng EM. Efficacy and safety of atomoxetine for attention-deficit/hyperactivity disorder in children and adolescents: meta-analysis and meta-regression analysis. *Psychopharmacology (Berl).* 2007;194:197–209.
6. Chamberlain SR, Del Campo N, Dowson J, et al. Atomoxetine improved response inhibition in adults with attention deficit/hyperactivity disorder. *Biol Psychiatry.* 2007;62:977–984.
7. Shelton RC. The dual-action hypothesis: does pharmacology matter? *J Clin Psychiatry.* 2004;65(suppl 17):5–10.
8. Schou M, Halldin C, Sovago J, et al. PET evaluation of novel radiofluorinated reboxetine analogs as norepinephrine transporter probes in the monkey brain. *Synapse.* 2004;53:57–67.
9. Seneca N, Andree B, Sjoholm N, et al. Whole-body biodistribution, radiation dosimetry estimates for the PET norepinephrine transporter probe (S,S)-[^{18}F]FMeNER-D2 in non-human primates. *Nucl Med Commun.* 2005;26:695–700.
10. Takano A, Gulyas B, Varrone A, et al. Imaging the norepinephrine transporter with positron emission tomography: initial human studies with (S,S)-[^{18}F]FMeNER-D_2. *Eur J Nucl Med Mol Imaging.* 2008;35:153–157.
11. Takano A, Halldin C, Varrone A, et al. Biodistribution and radiation dosimetry of the norepinephrine transporter radioligand (S,S)-[^{18}F]FMeNER-D_2: a human whole-body PET study. *Eur J Nucl Med Mol Imaging.* 2008;35:630–636.
12. Seneca N, Gulyas B, Varrone A, et al. Atomoxetine occupies the norepinephrine transporter in a dose-dependent fashion: a PET study in nonhuman primate brain using (S,S)-[^{18}F]FMeNER-D2. *Psychopharmacology (Berl).* 2006;188:119–127.
13. Innis RB, Cunningham VJ, Delforge J, et al. Consensus nomenclature for in vivo imaging of reversibly binding radioligands. *J Cereb Blood Flow Metab.* 2007;27:1533–1539.
14. Schou M, Halldin C, Pike VW, et al. Post-mortem human brain autoradiography of the norepinephrine transporter using (S,S)-[^{18}F]FMeNER-D2. *Eur Neuropsychopharmacol.* 2005;15:517–520.
15. Donnan GA, Kaczmarczyk SJ, Paxinos G, et al. Distribution of catecholamine uptake sites in human brain as determined by quantitative [^{3}H] mazindol autoradiography. *J Comp Neurol.* 1991;304:419–434.
16. Logan J, Wang GJ, Telang F, et al. Imaging the norepinephrine transporter in humans with (S,S)-[^{11}C]O-methyl reboxetine and PET: problems and progress. *Nucl Med Biol.* 2007;34:667–679.
17. Ito H, Sudo Y, Suhara T, Okubo Y, Halldin C, Farde L. Error analysis for quantification of [^{11}C]FLB 457 binding to extrastriatal D_2 dopamine receptors in the human brain. *Neuroimage.* 2001;13:531–539.
18. Lammertsma AA, Hume SP. Simplified reference tissue model for PET receptor studies. *Neuroimage.* 1996;4:153–158.
19. Ichise M, Liow JS, Lu JQ, et al. Linearized reference tissue parametric imaging methods: application to [^{11}C]DASB positron emission tomography studies of the serotonin transporter in human brain. *J Cereb Blood Flow Metab.* 2003;23:1096–1112.
20. Ordway GA, Stockmeier CA, Cason GW, Klimek V. Pharmacology and distribution of norepinephrine transporters in the human locus coeruleus and raphe nuclei. *J Neurosci.* 1997;17:1710–1719.
21. Lundberg J, Odano I, Olsson H, Halldin C, Farde L. Quantification of ^{11}C-MADAM binding to the serotonin transporter in the human brain. *J Nucl Med.* 2005;46:1505–1515.
22. Farde L, Ito H, Swahn CG, Pike VW, Halldin C. Quantitative analyses of carbonyl-carbon-11-WAY-100635 binding to central 5-hydroxytryptamine-1A receptors in man. *J Nucl Med.* 1998;39:1965–1971.
23. Takano A, Suzuki K, Kosaka J, et al. A dose-finding study of duloxetine based on serotonin transporter occupancy. *Psychopharmacology (Berl).* 2006;185:395–399.
24. Arakawa R, Ito H, Takano A, et al. Dose-finding study of paliperidone ER based on striatal and extrastriatal dopamine D_2 receptor occupancy in patients with schizophrenia. *Psychopharmacology (Berl).* 2008;197:229–235.

Quantitative Analysis of NK_1 Receptor in the Human Brain Using PET with ^{18}F-FE-SPA-RQ

Masaki Okumura[1,2], Ryosuke Arakawa[1,2], Hiroshi Ito[1], Chie Seki[1], Hidehiko Takahashi[1], Harumasa Takano[1], Eisuke Haneda[1,3], Ryuji Nakao[4], Hidenori Suzuki[3], Kazutoshi Suzuki[4], Yoshiro Okubo[2], and Tetsuya Suhara[1]

[1]Molecular Neuroimaging Group, Molecular Imaging Center, National Institute of Radiological Sciences, Chiba, Japan; [2]Department of Neuropsychiatry, Nippon Medical School, Tokyo, Japan; [3]Department of Pharmacology, Nippon Medical School, Tokyo, Japan; and [4]Molecular Probe Group, Molecular Imaging Center, National Institute of Radiological Sciences, Chiba, Japan

^{18}F-fluoroethyl-SPA-RQ (^{18}F-FE-SPA-RQ) was recently developed as a radioligand for the measurement of neurokinin 1 (NK_1) receptor with PET. In this study, we used ^{18}F-FE-SPA-RQ with PET to visualize and quantify NK_1 receptor in the human brain. **Methods:** PET scans were performed on 7 healthy men after intravenous injection of ^{18}F-FE-SPA-RQ. Binding potential (BP_{ND}) was calculated by the indirect kinetic, simplified reference tissue model (SRTM), and ratio methods. The indirect kinetic method was used as the gold standard method and was compared with the SRTM method, with scan times of 180, 270, and 330 min, and with the ratio method, with time integration intervals of 120–180, 210–270, and 300–330 min. The cerebellum was used as the reference brain region. **Results:** Regional radioactivity was highest in the caudate head and putamen; mid level in the parahippocampus, cerebral cortex, and thalamus; and lowest in the cerebellum. BP_{ND} values by the indirect kinetic method were 3.15 ± 0.36, 3.11 ± 0.66, 1.17 ± 0.25, and 0.46 ± 0.14 in the caudate, putamen, parahippocampal region, and thalamus, respectively. For cerebral cortical regions, BP_{ND} values by the indirect kinetic method were 0.94 ± 0.23, 0.82 ± 0.15, 0.76 ± 0.15, and 0.69 ± 0.16 in the occipital, temporal, frontal, and anterior cingulate cortices, respectively. BP_{ND} values by the SRTM and ratio methods were in good agreement with those by the indirect kinetic method (r = 0.94–0.98). **Conclusion:** The regional distribution of ^{18}F-FE-SPA-RQ was in agreement with previous PET studies and postmortem studies of NK_1 receptor in the human brain. The ratio method will be useful for clinical research of psychiatric disorders, for the estimation of NK_1 receptor without arterial blood sampling and long dynamic PET.

Key Words: NK_1 receptor; substance P; ^{18}F-FE-SPA-RQ; PET; human brain

J Nucl Med 2008; 49:1749–1755
DOI: 10.2967/jnumed.108.054353

Tachykinins are a family of neuropeptides that serve as neurotransmitters in the central nervous system (CNS) and peripheral nervous system (PNS). Three major mammalian tachykinins—substance P (SP), neurokinin A, and neurokinin B—are known, and they share a consensus amino acid sequence (-Phe-X-Gly-Leu-Met-NH_2) in their carboxyl terminals (*1–4*). SP is a well-characterized neuropeptide, participating in neurotransmission by itself or synergistically with other neurotransmitters such as monoamines, acetylcholine, and glutamate in nerve terminals. Receptors for tachykinins—termed neurokinin 1 (NK_1), NK_2, and NK_3 receptors—have been identified (all are G protein–coupled 7-transmembrane receptors) and demonstrated to selectively show high affinity for SP, neurokinin A, and neurokinin B, respectively (*5,6*). NK_1 receptors are expressed in both CNS and PNS, whereas NK_2 and NK_3 receptors are expressed in PNS and CNS, respectively (*7,8*). SP and NK_1 receptors have been shown to play significant roles in pain (*9*), emesis (*10*), neuroinflammation (*11,12*), vasomotor control, and many gastrointestinal functions. Because the SP–NK_1 system is localized in brain regions (such as the striatum, amygdala, hypothalamus, raphe nucleus, and periaqueductal gray matter) that are involved in the regulation of affective behavior (*7,8*), the activity of the central tachykinergic pathway mediated by SP and NK_1 receptors is conceived to be mechanistically related to psychiatric conditions such as depression and anxiety disorder. Recent clinical trials of the NK_1 receptor antagonist aprepitant have shown that the blockade of SP is a highly effective strategy for the prevention of chemotherapy-induced nausea and vomiting (*13–15*). Aprepitant was recently registered worldwide, and it represents an improvement for antiemetic control during chemotherapy. Early clinical studies also suggested that aprepitant may have antidepressant activity, implicating SP in the modulation of mood and anxiety in humans (*16,17*). However, recent results from phase III clinical trials indicate that aprepitant is not effective for the treatment of depression (*18*).

A recently developed nonpeptide PET tracer that can permeate the blood–brain barrier, [^{18}F-2-fluoromethoxy-5-(5-trifluoromethyl-tetrazol-1-yl)-benzyl]([2S,3S]2-phenyl-piperidin-3-yl)-amine) (^{18}F-SPA-RQ) (*19*), has been proven

Received May 14, 2008; revision accepted Jul. 14, 2008.
For correspondence or reprints contact: Hiroshi Ito, Molecular Neuroimaging Group, Molecular Imaging Center, National Institute of Radiological Sciences 4-9-1, Anagawa, Inage-ku, Chiba, 263-8555, Japan.
E-mail: hito@nirs.go.jp

to bind to NK_1 receptors with high affinity and selectivity and applied to in vivo imaging of human brains (*20–22*).

^{18}F-fluoroethyl-SPA-RQ (^{18}F-FE-SPA-RQ) was recently developed as a radioligand for the measurement of NK_1 receptors (*23*). It is the fluoroethyl analog of ^{18}F-SPA-RQ and was designed for brain imaging with reduced radioactive accumulation in bone by slowing the rate of defluorination. ^{18}F-FE-SPA-RQ has higher affinity for NK_1 receptors than does ^{18}F-SPA-RQ (human NK_1 inhibitory concentration of 50% [IC_{50}] = 17 and 67 pM for ^{18}F-FE-SPA-RQ and ^{18}F-SPA-RQ, respectively), and a small-animal PET study has been performed using ^{18}F-FE-SPA-RQ (*24*). In the present study, we aimed to quantify NK_1 receptor binding in the human brain using ^{18}F-FE-SPA-RQ with arterial blood sampling and also to validate noninvasive methods for the quantification without arterial blood sampling.

MATERIALS AND METHODS

Subjects

A total of 7 healthy male subjects (age range, 20–31 y; mean ± SD, 24.6 ± 4.0 y) participated in this study. All subjects were free of any somatic, neurologic, or psychiatric disorders, and they had no history of current or previous drug abuse. After we described the study to the participants, written informed consent was obtained. The study was approved by the Ethics and Radiation Safety Committee of the National Institute of Radiologic Sciences, Chiba, Japan.

Radioligand

The NK_1 receptor antagonist SPA-RQ (molecular weight, 450M) was labeled with the positron emitter ^{18}F (half-life, 109.8 min). Details of the precursor compound, radiosynthesis, and quality control were described previously (*23,25*). Briefly, ^{18}F-FCH_2CH_2Br was prepared from ^{18}F-F^- and 2-bromoethyl triflate and purified by distillation. ^{18}F-Fluoroalkylation of the deprotonated phenolic hydroxyl group in the precursor with FCH_2CH_2Br in dimethyl formamide was performed at 120°C for 10 min. The resultant ^{18}F-FE-SPA-RQ was purified by preparative high-performance liquid chromatography (HPLC). The final product was formulated in saline solution (10 mL) containing polysorbate 80 (75 μL).

PET Procedure

A PET scanner system (ECAT EXACT HR+; CTI-Siemens) was used for all subjects, and a head restraint was used to minimize head movement. A transmission scan for attenuation correction was performed using a ^{68}Ge–^{68}Ga source, and a dynamic PET scan was performed after a 1-min intravenous slow-bolus injection of 210.2–228.8 MBq (221.6 ± 6.7 MBq) of ^{18}F-FE-SPA-RQ. Specific radioactivity of ^{18}F-FE-SPA-RQ was 281.8–487.7 GBq/μmol (355.6 ± 68.7 GBq/μmol). Brain radioactivity was measured from 0 to 90 min (1 min × 10, 2 min × 15, 5 min × 10), from 120 to 180 min (5 min × 12), from 210 to 270 min (5 min × 12), and from 300 to 330 min (5 min × 6). MR images of the brain were acquired with a 1.5-T MRI scanner (Gyroscan NT; Philips). T1-weighted images were obtained at 1-mm slices.

Arterial Blood Sampling and Metabolite Analysis

To obtain the arterial input function, arterial blood samples were taken manually 49 times during PET. Each of the blood samples was centrifuged to obtain plasma and blood cell fractions, and the concentrations of radioactivity in whole blood and in plasma were measured.

The percentage of unchanged ^{18}F-FE-SPA-RQ in plasma was determined by HPLC in 29 of the total blood samples. Acetonitrile was added to each plasma sample, and samples were centrifuged. The supernatant was subjected to radio-HPLC analysis using an XBridge Prep C18 column (Waters) (mobile phase, 6:4 90% acetonitrile:50 mM phosphoric acid). The plasma input function was defined as the radioactivity of plasma multiplied by the percentage of unchanged radioligand. Plasma protein binding was not determined in the present study.

Regions of Interest

All MR images were coregistered to the PET images using a statistical parametric mapping (SPM2) system. Regions of interest were drawn manually on summated PET images with reference to coregistered MRI and were defined for the caudate head; putamen; parahippocampal region; occipital, temporal, frontal, and anterior cingulate cortices; thalamus; and cerebellum, according to our previous study (*26*). The parahippocampal region included the hippocampus, posterior part of the parahippocampal gyrus, and uncus including the amygdala. Regional radioactivity was calculated for each frame, corrected for decay, and plotted versus time.

Kinetics Model of ^{18}F-FE-SPA-RQ

The 3-compartment model (3CM) with 4 first-order rate constants was used to describe the kinetics of ^{18}F-FE-SPA-RQ in the brain. The 3 compartments were defined as follows: C_P, the radioactivity concentration of unchanged radioligand in plasma (arterial input function); C_{ND}, the radioactivity concentration of nondisplaceable radioligand in the brain, including nonspecifically bound and free radioligand; and C_S, the radioactivity concentration of radioligand specifically bound to receptors. The rate constants K_1 and k_2 represent the influx and efflux rates for radioligand diffusion through the blood–brain barrier, respectively. The rate constants k_3 and k_4 are the radioligand transfers between the compartments for nondisplaceable and specifically bound radioligand. This model can be described by the following equations:

$$dC_{ND}(t)/dt = K_1C_P(t) - (k_2 + k_3)C_{ND}(t) + k_4C_S(t),$$

$$dC_S(t)/dt = k_3C_{ND}(t) - k_4C_S(t), \text{ and}$$

$$C_T(t) = C_{ND}(t)+C_S(t).$$

$C_T(t)$ is the total radioactivity concentration in a brain region measured by PET.

Calculation of ^{18}F-FE-SPA-RQ Binding Potential (BP_{ND})

^{18}F-FE-SPA-RQ binding was quantified by the indirect kinetic, simplified reference tissue model (SRTM), and ratio methods. In these methods, ^{18}F-FE-SPA-RQ bindings were expressed as BP_{ND} relative to nondisplaceable bindings (*27*). We used the cerebellum as reference brain region because of its negligible NK_1 receptor

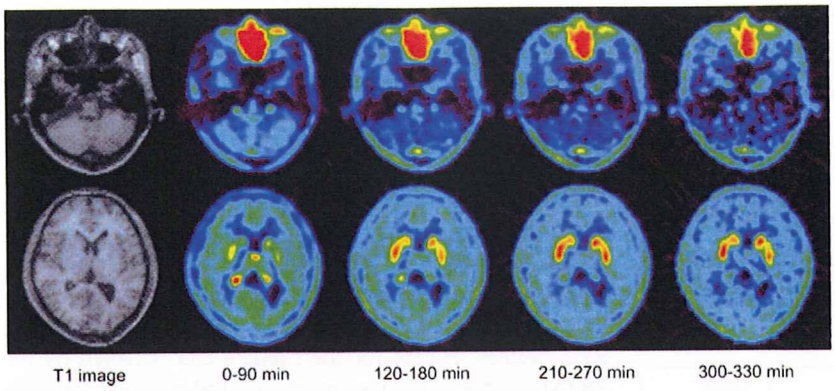

FIGURE 1. Typical summated PET images of ^{18}F-FE-SPA-RQ and T1-weighted MR images. Upper row shows slice of cerebellum, and lower row shows slice of caudate, putamen, and cerebral cortex.

density (*20,22,28*). For these analyses, the software package PMOD (PMOD Technologies) was used.

Indirect Kinetic Method. With the cerebellum as reference region, BP_{ND} can be expressed as:

$$BP_{ND} = V_{T(regions)}/V_{T(cerebellum)} - 1,$$

where $V_{T(regions)}$ is the total distribution volume ($= [K_1/k_2][k_3/k_4 + 1]$) of target regions and $V_{T(cerebellum)}$ is that of the cerebellum. K_1, k_2, k_3, and k_4 values were determined by nonlinear least-squares curve fitting to the regional time–activity curves. In this analysis, blood volume (V_b), which depends on the first-pass extraction fraction of the tracer, was assumed to be 0.04 mL/mL, with use of the radioactivity of whole blood to diminish the influence of the tracer remaining in the blood. In this study, the indirect kinetic method was used as the gold standard method (*29*).

SRTM Method. Assuming that both target and reference regions have the same level of nondisplaceable binding, the SRTM can be used to describe time–activity data in the target region as follows (*30*):

$$C_T(t) = R_1C_R(t) + (k_2 - R_1k_2/[1+BP_{ND}])C_R(t)* \exp(-k_2t/[1+BP_{ND}]),$$

where R_1 is the ratio of K_1/K_1' (K_1, influx rate constant for the brain region; K_1', influx rate constant for the reference region), $C_R(t)$ is the radioactivity concentration in the reference region (cerebellum), and * denotes the convolution integral. Using this method, 3 parameters (R_1, k_2, and BP_{ND}) were estimated by a nonlinear curve-fitting procedure. Scan data up to 180, 270, and 330 min were used.

Ratio Method. In the ratio method, BP_{ND} can be expressed as:

$$BP_{ND} = AUC_{(regions)}/AUC_{(cerebellum)} - 1,$$

where $AUC_{(regions)}$ is the area under the time–activity curve of target regions and $AUC_{(cerebellum)}$ is the time–activity curve of the cerebellum. The integration intervals of 120–180, 210–270, and 300–330 min were used.

RESULTS

Typical summated PET images of 4 time periods and T1-weighted MR images are shown in Figure 1. Typical time–activity curves in the brain showed that regional radioactivity was highest in the putamen and caudate (Fig. 2). The next highest region was the parahippocampus, followed by the cerebral cortices and thalamus. Among cerebral

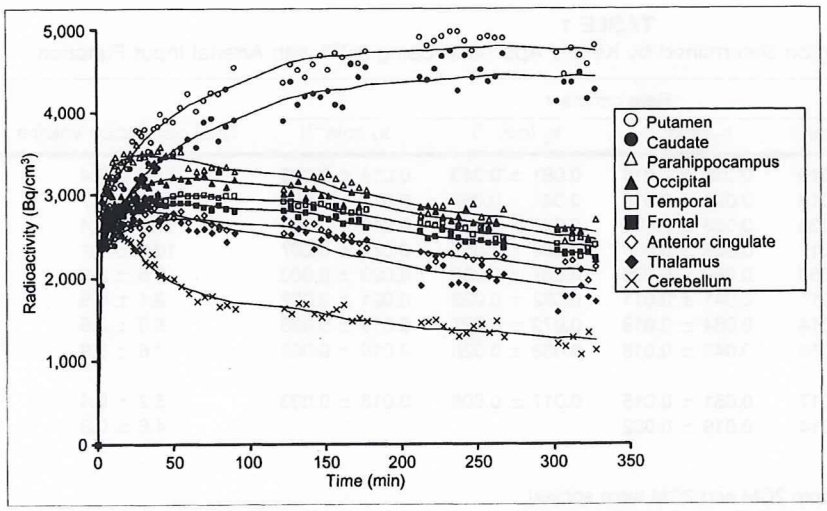

FIGURE 2. Typical time–activity curves of ^{18}F-FE-SPA-RQ in brain. Time–activity curves of all regions could be described by 3CM.

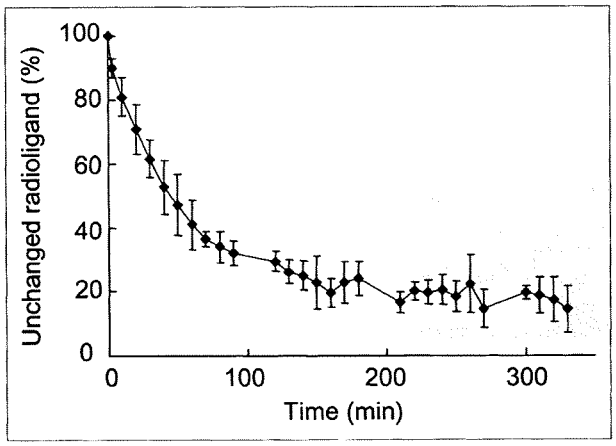

FIGURE 3. Average percentage of unchanged ^{18}F-FE-SPA-RQ in plasma. Bars indicate 1 SD.

cortices, the occipital cortex showed the highest radioactivity. Lowest radioactivity was shown in the cerebellum.

In this study, the fraction of unchanged ^{18}F-FE-SPA-RQ in plasma could not be measured by HPLC analysis in 3 of the 7 subjects because of low radioactivity in blood samples. So, the average of the fractions of unchanged ^{18}F-FE-SPA-RQ in plasma of the other 4 subjects was used for these 3 subjects for the indirect kinetic method. The average percentage fraction of unchanged ^{18}F-FE-SPA-RQ in plasma of the 4 subjects was 90.0% ± 2.9% at 3 min, 80.9% ± 6.1% at 10 min, 32.0% ± 3.9% at 90 min, 23.9% ± 5.3% at 180 min, 14.6% ± 5.9% at 270 min, and 14.4% ± 7.3% at 330 min (Fig. 3).

The rate constants for the 9 regions determined by the kinetic approach using the 3CM with arterial input function are shown in Table 1. For the cerebellum, the 2-compartment model (2CM) without specific binding compartment was also used. Akaike information criteria of the 3CM were significantly lower than those of the 2CM in the cerebellum (290 ± 28 vs. 409 ± 25, $P < 0.0001$; paired t statistics).

The BP_{ND} values of all brain regions calculated by all methods are shown in Table 2. BP_{ND} values by the SRTM method with a scan time of 330 min showed the best correlation with those by the indirect kinetic method (r = 0.98) (Fig. 4A). The SRTM method with scan times of 270 and 180 min and the ratio method with time integration intervals of 300–330, 210–270, and 120–180 min were also in good agreement with the indirect kinetic method in BP_{ND} values (r = 0.94–0.97) (Figs. 4B and 4C; Fig. 5). The BP_{ND} values, except for the caudate and putamen by the SRTM method with a scan time of 180 min and the ratio method with a time integration interval of 120–180 min, were also in good agreement with the indirect kinetic method (SRTM, r = 0.94, $y = 0.70x + 0.20$; ratio method, r = 0.94, $y = 0.69x + 0.20$).

The BP_{ND} values determined by the kinetic approach ($= k_3/k_4$) were 4.39 ± 3.93 and 5.94 ± 3.44 in the caudate and putamen. Those in the other regions were much smaller and varied widely.

DISCUSSION

After the intravenous injection of ^{18}F-FE-SPA-RQ, radioactivity was highest in the caudate and putamen and lowest in the cerebellum. BP_{ND} values in the caudate and putamen by the indirect kinetic method were 3.15 ± 0.36 and 3.11 ± 0.66, respectively, almost the same as in the previous human PET study with ^{18}F-SPA-RQ (3.08 ± 0.48 in the caudate and 3.71 ± 1.00 in the putamen) (*22*). The parahippocampal region and cerebral cortices showed moderate uptake, and the occipital cortex showed the highest uptake among the cerebral cortices. The thalamus showed relatively low uptake. The uptake shown in these regions was almost the same order of progression as the uptake in previous human PET studies with ^{18}F-SPA-RQ and autoradiographic studies of the human postmortem brain

TABLE 1
Rate Constants for Each Brain Region Determined by Kinetic Approach Using 3CM with Arterial Input Function

Region	Rate constant				Total distribution volume
	K_1 (mL/mL/min)	k_2 (min^{-1})	k_3 (min^{-1})	k_4 (min^{-1})	
Putamen	0.111 ± 0.019	0.036 ± 0.016	0.081 ± 0.040	0.014 ± 0.003	21.3 ± 3.4
Caudate	0.088 ± 0.018	0.023 ± 0.018	0.061 ± 0.067	0.011 ± 0.005	21.5 ± 1.7
Parahippocampus	0.140 ± 0.023	0.033 ± 0.007	0.027 ± 0.020	0.015 ± 0.006	11.3 ± 1.4
Occipital lobe	0.127 ± 0.017	0.065 ± 0.038	0.089 ± 0.057	0.021 ± 0.007	10.0 ± 1.1
Temporal lobe	0.106 ± 0.050	0.050 ± 0.025	0.067 ± 0.038	0.020 ± 0.003	9.5 ± 0.9
Frontal lobe	0.108 ± 0.011	0.041 ± 0.011	0.052 ± 0.023	0.021 ± 0.002	9.1 ± 0.9
Anterior cingulate cortex	0.115 ± 0.014	0.064 ± 0.018	0.072 ± 0.027	0.019 ± 0.005	8.8 ± 0.9
Thalamus	0.112 ± 0.019	0.043 ± 0.018	0.038 ± 0.026	0.019 ± 0.003	7.6 ± 0.9
Cerebellum					
3CM	0.115 ± 0.017	0.051 ± 0.015	0.017 ± 0.008	0.013 ± 0.003	5.2 ± 0.4
2CM	0.089 ± 0.014	0.019 ± 0.002			4.6 ± 0.3

Values are mean ± SD. For cerebellum, both 2CM and 3CM were applied.

TABLE 2
BP_{ND} Values for Each Brain Region with All Methods

Region	Method						
		SRTM (min)			Ratio (min)		
	Indirect kinetic	330	270	180	300–330	210–270	120–180
Putamen	3.11 ± 0.66	2.43 ± 0.33	2.33 ± 0.32	2.20 ± 0.27	2.62 ± 0.40	2.25 ± 0.28	1.81 ± 0.19
Caudate	3.15 ± 0.36	2.14 ± 0.24	2.02 ± 0.22	1.91 ± 0.20	2.31 ± 0.40	1.98 ± 0.26	1.57 ± 0.17
Parahippocampus	1.17 ± 0.25	1.04 ± 0.16	1.02 ± 0.12	1.01 ± 0.12	1.11 ± 0.22	1.05 ± 0.16	1.03 ± 0.20
Occipital lobe	0.94 ± 0.23	0.88 ± 0.14	0.92 ± 0.07	0.90 ± 0.13	0.97 ± 0.16	0.94 ± 0.16	0.95 ± 0.17
Temporal lobe	0.82 ± 0.15	0.77 ± 0.11	0.79 ± 0.08	0.78 ± 0.11	0.85 ± 0.15	0.83 ± 0.15	0.79 ± 0.15
Frontal lobe	0.76 ± 0.15	0.72 ± 0.12	0.74 ± 0.07	0.73 ± 0.11	0.79 ± 0.17	0.76 ± 0.15	0.75 ± 0.15
Anterior cingulate cortex	0.69 ± 0.16	0.66 ± 0.15	0.67 ± 0.13	0.71 ± 0.17	0.70 ± 0.16	0.69 ± 0.13	0.67 ± 0.13
Thalamus	0.46 ± 0.14	0.46 ± 0.13	0.51 ± 0.10	0.49 ± 0.14	0.45 ± 0.12	0.45 ± 0.13	0.49 ± 0.16

Values are mean ± SD.

(*20,22,28*). In a previous autoradiographic study using ^{3}H-GR205171, the maximum number of binding sites for NK_1 receptor in the striatum was 6 times as much as in the cortex (*31*), a result in accordance with the BP_{ND} values in these regions in the present study.

In this study, the indirect kinetic method with arterial blood sampling was used as the gold standard method, because BP_{ND} determined by the kinetic approach as k_3/k_4 showed wide variation. The BP_{ND} values in all brain regions determined by the SRTM method (with scan times of 330, 270, and 180 min) and by the ratio method (with time integration intervals of 300–330, 210–270, and 120–180 min) were in good agreement with those determined by the indirect kinetic method. Although good correlations were observed in BP_{ND} values among the methods, BP_{ND} was underestimated in the caudate and putamen using the

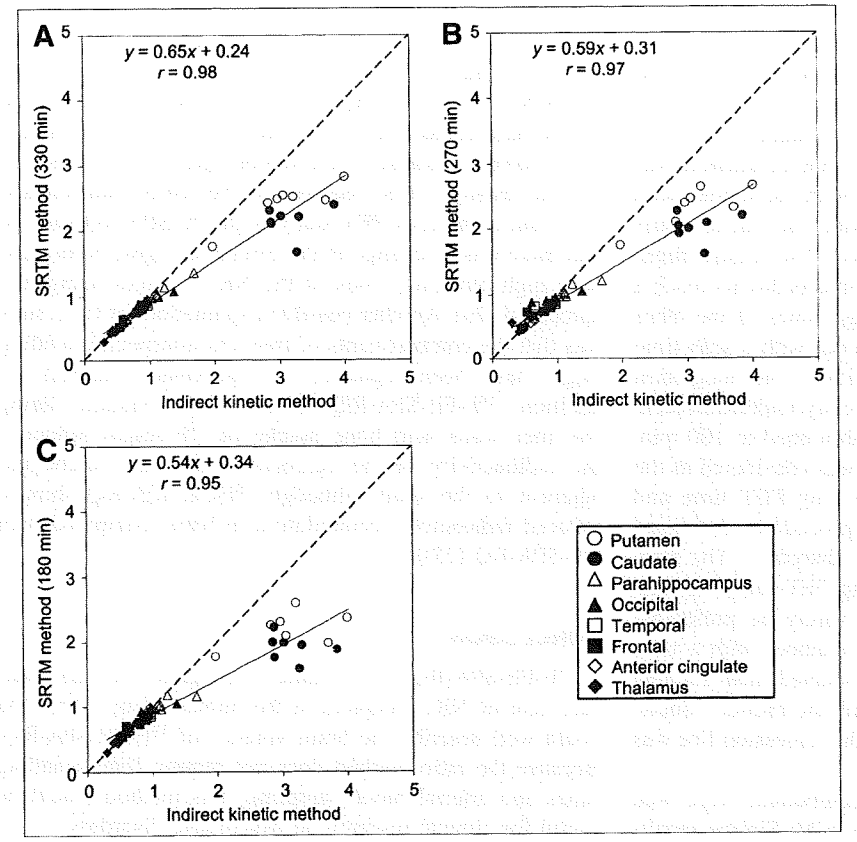

FIGURE 4. Correlation among BP_{ND} values in all brain regions estimated by indirect kinetic and SRTM methods, with scan times of 330 (A), 270 (B), and 180 (C) min.

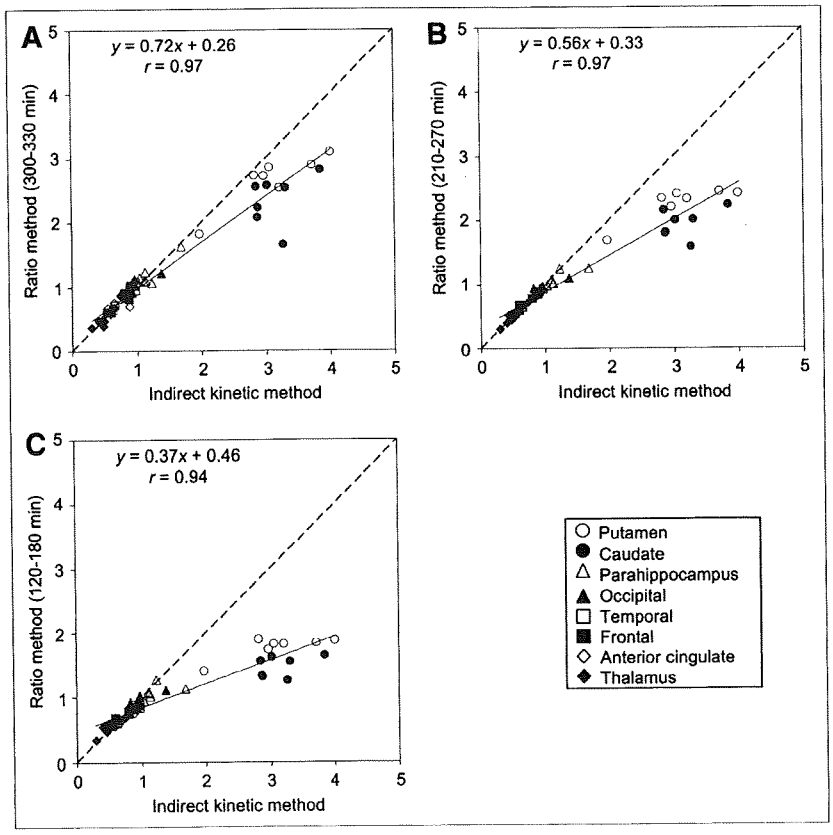

FIGURE 5. Correlation among BP_{ND} values in all brain regions estimated by indirect kinetic and ratio methods, with time integration intervals of 300–330 (A), 210–270 (B), and 120–180 (C) min.

SRTM and ratio methods. The underestimations of BP_{ND} were 32% and 34% in the caudate and 22% and 16% in the putamen for the SRTM method (with a scan time of 330 min) and the ratio method (with a time integration interval of 300–330 min), respectively. More underestimation was observed in the caudate and putamen with the shorter scan time in the SRTM method and with the earlier time integration interval in the ratio method. The reason might be that striatal radioactivity in some subjects did not reach a peak by 330 min. However, the BP_{ND} values of the other regions calculated by the SRTM method (with a scan time of 180 min) and the ratio method (with a time integration interval of 120–180 min) were not greatly underestimated, indicating that the scan time can be shortened to 180 min. Although the indirect kinetic method was considered as the gold standard method, it required a long PET time and arterial blood sampling, an invasive procedure sometimes difficult for patients with psychiatric disorders. The ratio method, which does not require a long PET scanning time and arterial blood sampling, would surely be preferable for clinical investigations. The ratio method, with a time integration interval of 300–330 min, seemed most suitable because the correlation coefficient with the indirect kinetic method was highest and the slope of the regression line was nearest to 1.

The time–activity curves in the cerebellum were well described by the 3CM rather than the 2CM. Similar results were reported for several PET radioligands, with the kinetics in the reference region also being evaluated using the 3CM (*29,32,33*). The results could be explained if the cerebellum would contain specific bindings for NK_1 receptors. However, previous autoradiographic studies showed that the density of NK_1 receptors in the cerebellum was low (*22*), and a previous PET study with ^{18}F-SPA-RQ showed that there was no change in the cerebellar signal before and after high blocking doses of the NK_1 receptor antagonist aprepitant (*20*). Another possible explanation for the results was that the compartments of free and nonspecific binding might have been separated by the kinetic analysis. In addition, ^{18}F-FE-SPA-RQ showed defluorination during the later scans, and bone uptake of ^{18}F might influence the radioactivity in the cerebral cortex and cerebellum adjacent to the skull (although ^{18}F-FE-SPA-RQ showed reduced radioactive accumulation in bone, compared with ^{18}F-SPA-RQ (*23*)).

CONCLUSION

^{18}F-FE-SPA-RQ is a suitable radioligand for PET measurement of NK_1 receptors in the human brain. The 3CM could well describe the brain kinetics of ^{18}F-FE-SPA-RQ. Because the ratio method does not require long scanning times and arterial blood sampling, this method would be useful for clinical research on psychiatric disorders.

ACKNOWLEDGMENTS

We thank Dr. Fumitoshi Kodaka, Dr. Tatsui Otsuka, Katsuyuki Tanimoto, Takahiro Shiraishi, and Akira Ando for their assistance in performing the PET experiments at the National Institute of Radiological Sciences. We also thank Yoshiko Fukushima of the National Institute of Radiological Sciences for her help as clinical research coordinator. This study was supported by a consignment expense for the Molecular Imaging Program on Research Base for PET Diagnosis from the Ministry of Education, Culture, Sports, Science and Technology (MEXT), Japanese Government.

REFERENCES

1. Baker KG, Halliday GM, Hornung JP, Geffen LB, Cotton RG, Tork I. Distribution, morphology and number of monoamine-synthesizing and substance P-containing neurons in the human dorsal raphe nucleus. *Neuroscience.* 1991; 42:757–775.
2. Nicholas AP, Pieribone VA, Arvidsson U, Hokfelt T. Serotonin-, substance P- and glutamate/aspartate-like immunoreactivities in medullo-spinal pathways of rat and primate. *Neuroscience.* 1992;48:545–559.
3. Sergeyev V, Hokfelt T, Hurd Y. Serotonin and substance P co-exist in dorsal raphe neurons of the human brain. *Neuroreport.* 1999;10:3967–3970.
4. Vincent SR, Satoh K, Armstrong DM, Panula P, Vale W, Fibiger HC. Neuropeptides and NADPH-diaphorase activity in the ascending cholinergic reticular system of the rat. *Neuroscience.* 1986;17:167–182.
5. Masu Y, Nakayama K, Tamaki H, Harada Y, Kuno M, Nakanishi S. cDNA cloning of bovine substance-K receptor through oocyte expression system. *Nature.* 1987;329:836–838.
6. Nakanishi S. Mammalian tachykinin receptors. *Annu Rev Neurosci.* 1991; 14:123–136.
7. Ding YQ, Shigemoto R, Takada M, Ohishi H, Nakanishi S, Mizuno N. Localization of the neuromedin K receptor (NK_3) in the central nervous system of the rat. *J Comp Neurol.* 1996;364:290–310.
8. Nakaya Y, Kaneko T, Shigemoto R, Nakanishi S, Mizuno N. Immunohistochemical localization of substance P receptor in the central nervous system of the adult rat. *J Comp Neurol.* 1994;347:249–274.
9. Snider WD, McMahon SB. Tackling pain at the source: new ideas about nociceptors. *Neuron.* 1998;20:629–632.
10. Sanger GJ. Neurokinin NK_1 and NK_3 receptors as targets for drugs to treat gastrointestinal motility disorders and pain. *Br J Pharmacol.* 2004;141:1303–1312.
11. Kincy-Cain T, Bost KL. Increased susceptibility of mice to Salmonella infection following in vivo treatment with the substance P antagonist, spantide II. *J Immunol.* 1996;157:255–264.
12. Metwali A, Blum AM, Elliott DE, Setiawan T, Weinstock JV. Cutting edge: hemokinin has substance P-like function and expression in inflammation. *J Immunol.* 2004;172:6528–6532.
13. Hesketh PJ, Van Belle S, Aapro M, et al. Differential involvement of neurotransmitters through the time course of cisplatin-induced emesis as revealed by therapy with specific receptor antagonists. *Eur J Cancer.* 2003; 39:1074–1080.
14. Hesketh PJ, Grunberg SM, Gralla RJ, et al. The oral neurokinin-1 antagonist aprepitant for the prevention of chemotherapy-induced nausea and vomiting: a multinational, randomized, double-blind, placebo-controlled trial in patients receiving high-dose cisplatin—the Aprepitant Protocol 052 Study Group. *J Clin Oncol.* 2003;21:4112–4119.
15. de Wit R, Herrstedt J, Rapoport B, et al. Addition of the oral NK1 antagonist aprepitant to standard antiemetics provides protection against nausea and vomiting during multiple cycles of cisplatin-based chemotherapy. *J Clin Oncol.* 2003;21:4105–4111.
16. Kramer MS, Cutler N, Feighner J, et al. Distinct mechanism for antidepressant activity by blockade of central substance P receptors. *Science.* 1998;281:1640–1645.
17. Kramer MS, Winokur A, Kelsey J, et al. Demonstration of the efficacy and safety of a novel substance P (NK_1) receptor antagonist in major depression. *Neuropsychopharmacology.* 2004;29:385–392.
18. Keller M, Montgomery S, Ball W, et al. Lack of efficacy of the substance p (neurokinin1 receptor) antagonist aprepitant in the treatment of major depressive disorder. *Biol Psychiatry.* 2006;59:216–223.
19. Solin O, Eskola O, Hamill TG, et al. Synthesis and characterization of a potent, selective, radiolabeled substance-P antagonist for NK_1 receptor quantitation: ([^{18}F]SPA-RQ). *Mol Imaging Biol.* 2004;6:373–384.
20. Bergstrom M, Hargreaves RJ, Burns HD, et al. Human positron emission tomography studies of brain neurokinin 1 receptor occupancy by aprepitant. *Biol Psychiatry.* 2004;55:1007–1012.
21. Hargreaves R. Imaging substance P receptors (NK_1) in the living human brain using positron emission tomography. *J Clin Psychiatry.* 2002;63(suppl 11):S18–S24.
22. Hietala J, Nyman MJ, Eskola O, et al. Visualization and quantification of neurokinin-1 (NK_1) receptors in the human brain. *Mol Imaging Biol.* 2005; 7:262–272.
23. Hamill T, Ryan C, Krause S, et al. The synthesis and in vivo characterization of [^{18}F]FESPARQ, a neurokinin-1 (NK_1) receptor PET ligand [abstract]. *J Labelled Comp Radiopharm.* 2003;46(suppl 1):S35.
24. Haneda E, Higuchi M, Maeda J, et al. In vivo mapping of substance P receptors in brains of laboratory animals by high-resolution imaging systems. *Synapse.* 2007;61:205–215.
25. Zhang MR, Maeda J, Furutsuka K, et al. [^{18}F]FMDAA1106 and [^{18}F]FE-DAA1106: two positron-emitter labeled ligands for peripheral benzodiazepine receptor (PBR). *Bioorg Med Chem Lett.* 2003;13:201–204.
26. Ito H, Takahashi H, Arakawa R, Takano H, Suhara T. Normal database of dopaminergic neurotransmission system in human brain measured by positron emission tomography. *Neuroimage.* 2008;39:555–565.
27. Innis RB, Cunningham VJ, Delforge J, et al. Consensus nomenclature for in vivo imaging of reversibly binding radioligands. *J Cereb Blood Flow Metab.* 2007;27:1533–1539.
28. Caberlotto L, Hurd YL, Murdock P, et al. Neurokinin 1 receptor and relative abundance of the short and long isoforms in the human brain. *Eur J Neurosci.* 2003;17:1736–1746.
29. Ito H, Sudo Y, Suhara T, Okubo Y, Halldin C, Farde L. Error analysis for quantification of [^{11}C]FLB 457 binding to extrastriatal D_2 dopamine receptors in the human brain. *Neuroimage.* 2001;13:531–539.
30. Lammertsma AA, Hume SP. Simplified reference tissue model for PET receptor studies. *Neuroimage.* 1996;4:153–158.
31. Griffante C, Carletti R, Andreetta F, Corsi M. [^{3}H]GR205171 displays similar NK_1 receptor binding profile in gerbil and human brain. *Br J Pharmacol.* 2006; 148:39–45.
32. Farde L, Ito H, Swahn CG, Pike VW, Halldin C. Quantitative analyses of carbonyl-carbon-11-WAY-100635 binding to central 5-hydroxytryptamine-1A receptors in man. *J Nucl Med.* 1998;39:1965–1971.
33. Lundberg J, Odano I, Olsson H, Halldin C, Farde L. Quantification of ^{11}C-MADAM binding to the serotonin transporter in the human brain. *J Nucl Med.* 2005;46:1505–1515.